COO-1195-231

MASTER

PRODUCTION OF NEUTRAL KAONS AND LAMBDAS FROM CHARGED KAON INTERACTIONS WITH COMPLEX NUCLEI

BY

DAVID LEE BANNER
B.S., Purdue University, 1964
M.S., University of Illinois, 1966

THESIS

Submitted in partial fulfillment of the requirements
for the degree of Doctor of Philosophy in Physics
in the Graduate College of the
University of Illinois at Urbana-Champaign, January, 1972

Urbana, Illinois

This research was supported in part by the
U.S. Atomic Energy Commission under Contract AT(11-1)-1195

DISTRIBUTION OF THIS DOCUMENT IS UNLIMITED

DISCLAIMER

This report was prepared as an account of work sponsored by an agency of the United States Government. Neither the United States Government nor any agency Thereof, nor any of their employees, makes any warranty, express or implied, or assumes any legal liability or responsibility for the accuracy, completeness, or usefulness of any information, apparatus, product, or process disclosed, or represents that its use would not infringe privately owned rights. Reference herein to any specific commercial product, process, or service by trade name, trademark, manufacturer, or otherwise does not necessarily constitute or imply its endorsement, recommendation, or favoring by the United States Government or any agency thereof. The views and opinions of authors expressed herein do not necessarily state or reflect those of the United States Government or any agency thereof.

DISCLAIMER

Portions of this document may be illegible in electronic image products. Images are produced from the best available original document.

COO-1195-231

PRODUCTION OF NEUTRAL KAONS AND LAMBDAS FROM CHARGED KAON INTERACTIONS WITH COMPLEX NUCLEI

BY

DAVID LEE BANNER
B.S., Purdue University, 1964
M.S., University of Illinois, 1966

NOTICE

This report was prepared as an account of work sponsored by the United States Government. Neither the United States nor the United States Atomic Energy Commission, nor any of their employees, nor any of their contractors, subcontractors, or their employees, makes any warranty, express or implied, or assumes any legal liability or responsibility for the accuracy, completeness or usefulness of any information, apparatus, product or process disclosed, or represents that its use would not infringe privately owned rights.

THESIS

Submitted in partial fulfillment of the requirements
for the degree of Doctor of Philosophy in Physics
in the Graduate College of the
University of Illinois at Urbana-Champaign, January, 1972

Urbana, Illinois

This research was supported in part by the
U.S. Atomic Energy Commission under Contract AT(11-1)-1195

DISTRIBUTION OF THIS DOCUMENT IS UNLIMITED

PRODUCTION OF NEUTRAL KAONS AND LAMBDAS FROM CHARGED KAON INTERACTIONS WITH COMPLEX NUCLEI

David Lee Banner, Ph.D.
Department of Physics
University of Illinois at Urbana-Champaign, 1972

Measurements of the cross sections for the production of neutral kaons with momenta $\gtrsim$ 400 MeV/c and lambdas with momenta $\gtrsim$ 700 MeV/c from charged kaon interactions incident at 850 MeV/c on carbon, aluminum, copper, tin, and lead were made at the Argonne National Laboratory Zero-Gradient Synchrotron.

The measurements were made in order to determine which complex nuclear targets produced the best "beams" of neutral kaons, for use in an experiment to observe the decay of neutral K mesons into $\pi^+\pi^-$.

The cross sections are presented, and models for fitting the data, involving $A^{1/3}$- and $A^{2/3}$-parameterizations, are discussed. The K^o and $\bar{K}^o$ cross sections are fit about equally well with an $A^{1/3}$- and $A^{2/3}$-parameterization.

Monte Carlo computer codes were written to see whether the experimental cross sections could be understood on the basis of a simple impulse approximation model. Relative cross sections computed with the Monte Carlo codes agree reasonably well, after experimental cuts were included, with the experimental cross sections for K^o and $\bar{K}^o$ production. The agreement is not very good for Λ production, but a possible explanation for the disagreement is discussed.

For a fixed-length target, 7 cm long, copper is found to be best for producing the most intense "beams" of neutral kaons and lambdas.

ACKNOWLEDGMENTS

It is hardly possible to properly acknowledge all the significant contributions that so many people have made to my learning experiences while a graduate student, and, directly or indirectly, to this thesis.

I am particularly indebted to my advisor, Professor Albert Wattenberg, for the advice and counsel he has given me since the beginning of my studies at the University of Illinois.

I wish to thank Professor James H. Smith, Professor L. J. Koester, Jr., and Dr. Michael Gormley for their assistance and for their hard work on the experiment.

I am especially grateful for the help and the cooperation of fellow graduate students Jim Frank and Siegbert Raither.

I appreciate the excellent work of Robert Cullum and David Eitelbach, in computer programming; Len Seward and Roger Taylor, in construction and maintenance of electronic equipment; Phil Schadt, David Fancher, and Doug Brash, in helping to run the experiment; and Paul Robison, in construction of experimental apparatus.

The friendship of my friends, and the love and encouragement of my parents have been invaluable during these years.

TABLE OF CONTENTS

LIST OF TABLES

LIST OF FIGURES

I. INTRODUCTION AND MOTIVATION

Physicists planning experiments to investigate the interactions or decays of K^o's and $\bar{K}^o$'s and of Λ^o's are faced immediately with questions of how to obtain these particles in the necessary quantities. Furthermore, it can be important to know, with some modest degree of precision, the point of origin of these neutral particles.

Specifically, in an experiment[1] which was recently completed at the Argonne National Laboratory Zero-Gradient Synchrotron, it was necessary to produce "beams" of neutral kaons which, at the time of production, were pure K^o or pure $\bar{K}^o$; and it was necessary to know where each neutral known detected by the apparatus was produced, to within ~5/32".

A rather convenient method for satisfying the first of these requirements is to use the charge-exchange reactions of K^+ or K^-:

$$K^+ + n \rightarrow K^o + p \ ;$$

$$K^- + p \rightarrow \bar{K}^o + n \ .$$

With a target full of "only" protons, i.e. a hydrogen target, it is technically very difficult to tell where the charge-exchange took place (unless that "target" is a bubble chamber--which presents other problems!); and a target full of "only" neutrons simply does not exist. Furthermore, the copious production of neutral kaons was, and often is, necessary. So, the use of higher yield nuclear targets appeared attractive.

By using thin wafers of some material like carbon or copper, sandwiched between thin scintillation counters, it was possible to localize the point of interaction to within the required limits. The charge-exchange could clearly occur for either the K^+'s, on the neutrons in the target nuclei, or the K^-'s, on the protons.

The questions for which there were not clear answers were, "Which target, or targets, would yield the K^o's and $\overline{K}^o$'s most copiously?" and, "How troublesome will be the 'competition' from reactions like K^- + nucleus $\rightarrow \Lambda^o$ + anything?"

This thesis is a presentation of results of target studies which were performed in order to answer the two questions above. Results will be presented on the cross sections for production of K^o's, $\overline{K}^o$'s, and Λ's from $K^{\pm}$'s incident on several different nuclear targets, relative to the production from carbon. Measurements of the production of $\overline{K}^o$'s and Λ's from K^-'s incident on hydrogen were also performed. These will be presented and used to estimate the overall detection efficiences of the experimental apparatus used. Then, absolute production cross sections are calculated assuming the efficiency is A-independent.

Also presented in this thesis are the results of two Monte Carlo codes, one for K^+ and one for K^-, which were written in an attempt to understand the experimental results.

II. EXPERIMENTAL MEASUREMENTS

A. Beam

This experiment was performed in Beam No. 42 of the Argonne National Laboratory Zero-Gradient Synchrotron. This beam line, the layout of which is shown in Figure 1, was designed to deliver an enriched beam of low-momentum charged kaons.

A ten-foot long parallel plate electrostatic separator was used to accomplish velocity selection of on-momentum charged kaons from other on-momentum particles in the beam with different masses and, therefore, different velocities. For optimum separation of the intensity peaks of the various types of particles in the beam, at the mass-momentum slit, the beam particles should have had a well-defined momentum at the entrance to the separator. Unfortunately, due to constraints imposed by the physical location of this beam, it was not optimally designed with respect to the separation stage, because momentum selection was not completed until after the beam had already passed through the separator. The first element in the beam, a 20X42[2] bending magnet, acted primarily as a momentum dispersing element. The second bending magnet, 20X30,[2] in conjunction with the mass-momentum slit located downstream, was the principal momentum-selecting component.

The last stage of this beam line, from the mass-momentum slit to the final focus, was unusual, also. The last three quadrupoles functioned neither as a quadrupole triplet nor, in a strict sense, as a field lens and a doublet. The most upstream of these three quadrupoles did aid in achieving greater acceptance in the horizontal plane than would have been possible in its absence, but its operation in conjunction with the last two quadrupoles and also with the 31 VI 47[2] bending magnet, which had some slight horizontal focusing influence due to its wedge shape, was difficult to deal with empirically.

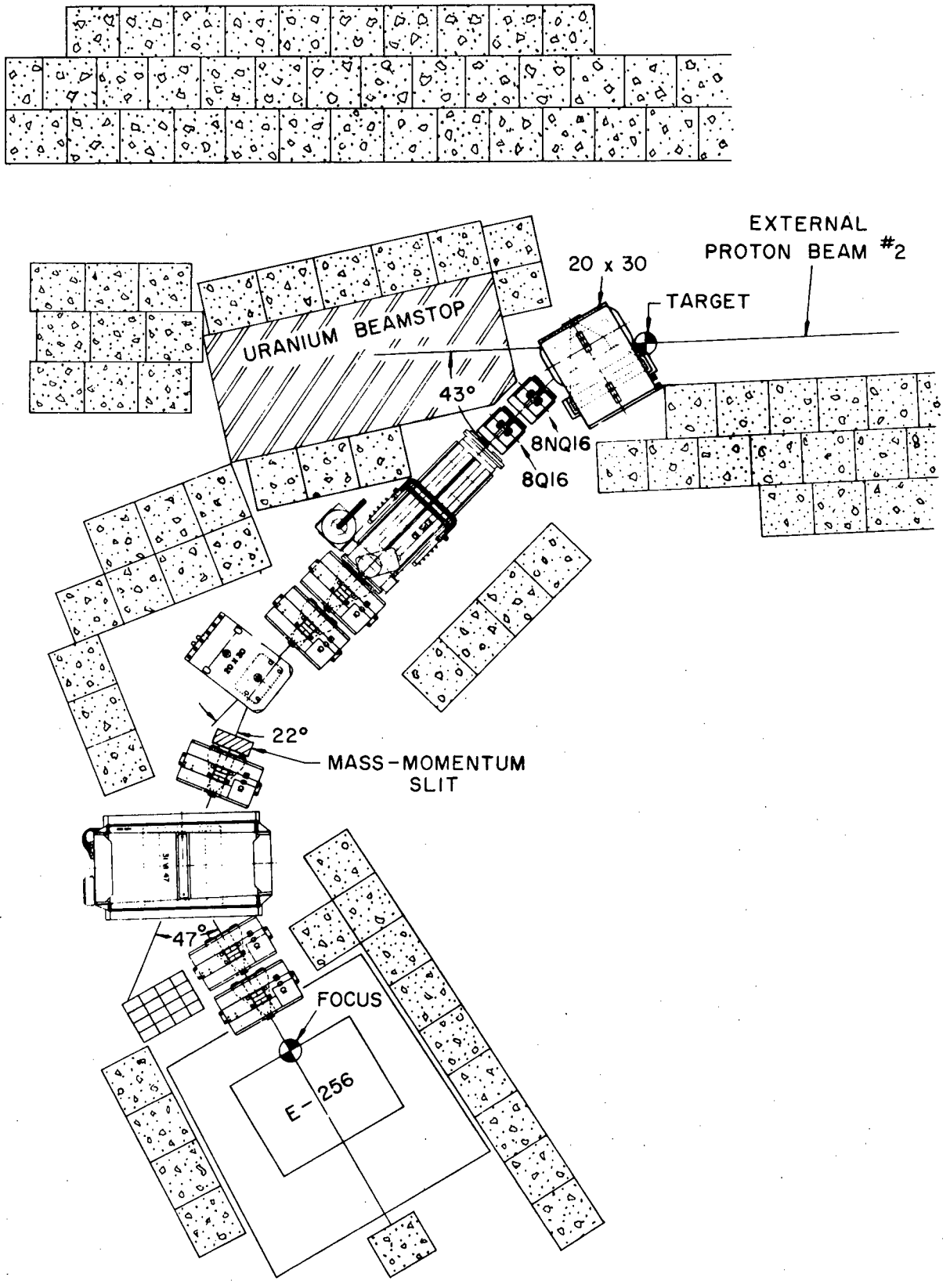
EXTERNAL
PROTON BEAM #2
20 x 30
TARGET
URANIUM BEAMSTOP
43°
8NQ16
8Q16
22°
MASS-MOMENTUM
SLIT
47°
FOCUS
E-256

Never-the-less, suitable values for the fields which were needed from each magnet in order to deliver a beam at the desired momentum for this experiment, 850 MeV/c, were not difficult to obtain. In general, the fields were computed using the well-known tracking and matching program TRAMP.[3]

In addition to the values computed using TRAMP, empirical settings were obtained for each of the three bending magnets using well-known wire-orbiting techniques.[4]

Details about the beam tuning procedure may be found in a report[5] prepared by Irwin Spirn and D. Banner. Also in that report are settings for each of the magnets used to deliver 800 MeV/c and 850 MeV/c beams, and the fluxes of particles measured at both those momenta.

B. Description of Apparatus

For descriptive clarity, it is convenient to consider the experimental apparatus in separate groups, according to function. These groups, in the order they will be described below, are event detection, range material, targets, event tracking, and event recording.

1. Event Detection

A typical event, of one of the types of interest in this experiment, is shown in Figure 2. In this event, a positively charged kaon in the beam charge-exchanged on a neutron to produce a K^o, which subsequently decayed into a π^+ and a π^-, and a proton which was stopped by the target material. How such an event was detected will be described in this section.

a. Cherenkov and Scintillation Counters

A top view of all the counters used for event detection is shown in Figure 3, superposed on the typical event. All of the counters were scintillation counters, except for the Cherenkov counter C_K. Counter B1 was placed at

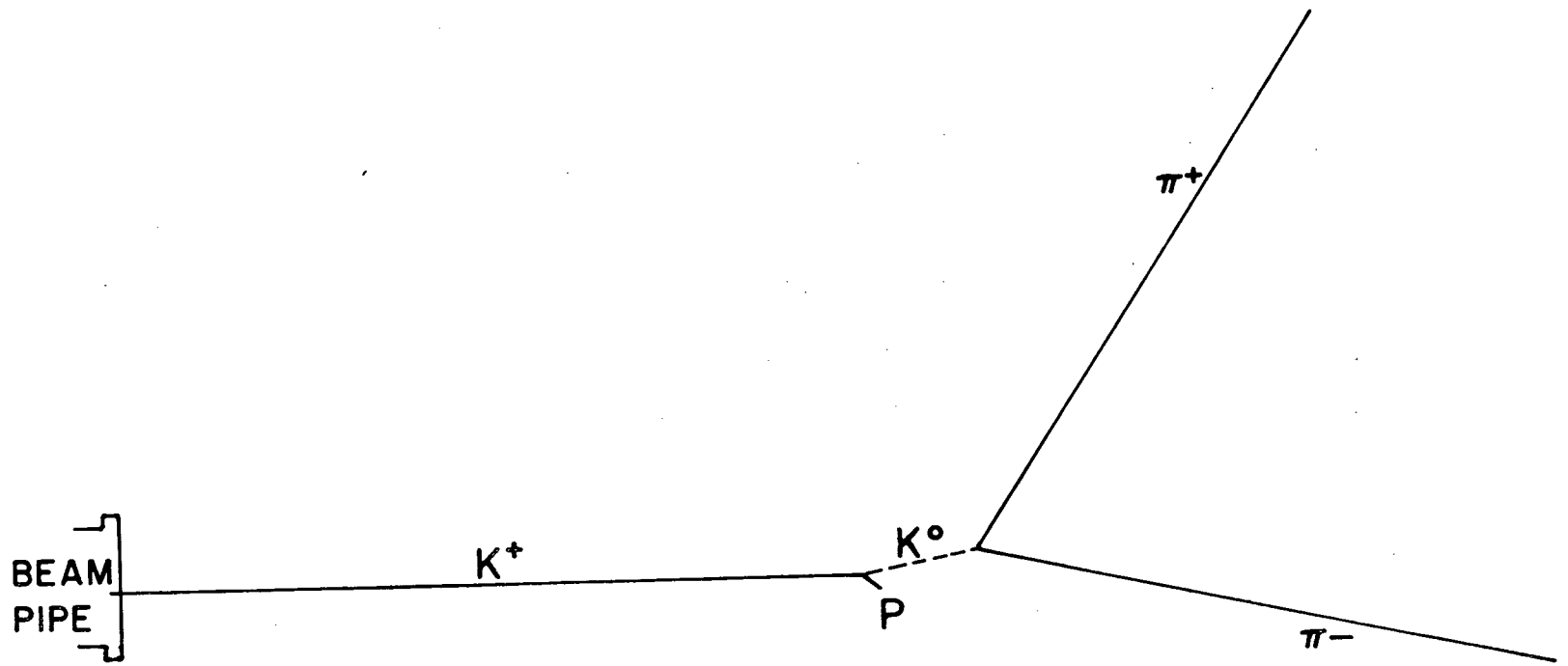

10"

Figure 3. A top view of the Cherenkov and scintillation counters and of the range material.

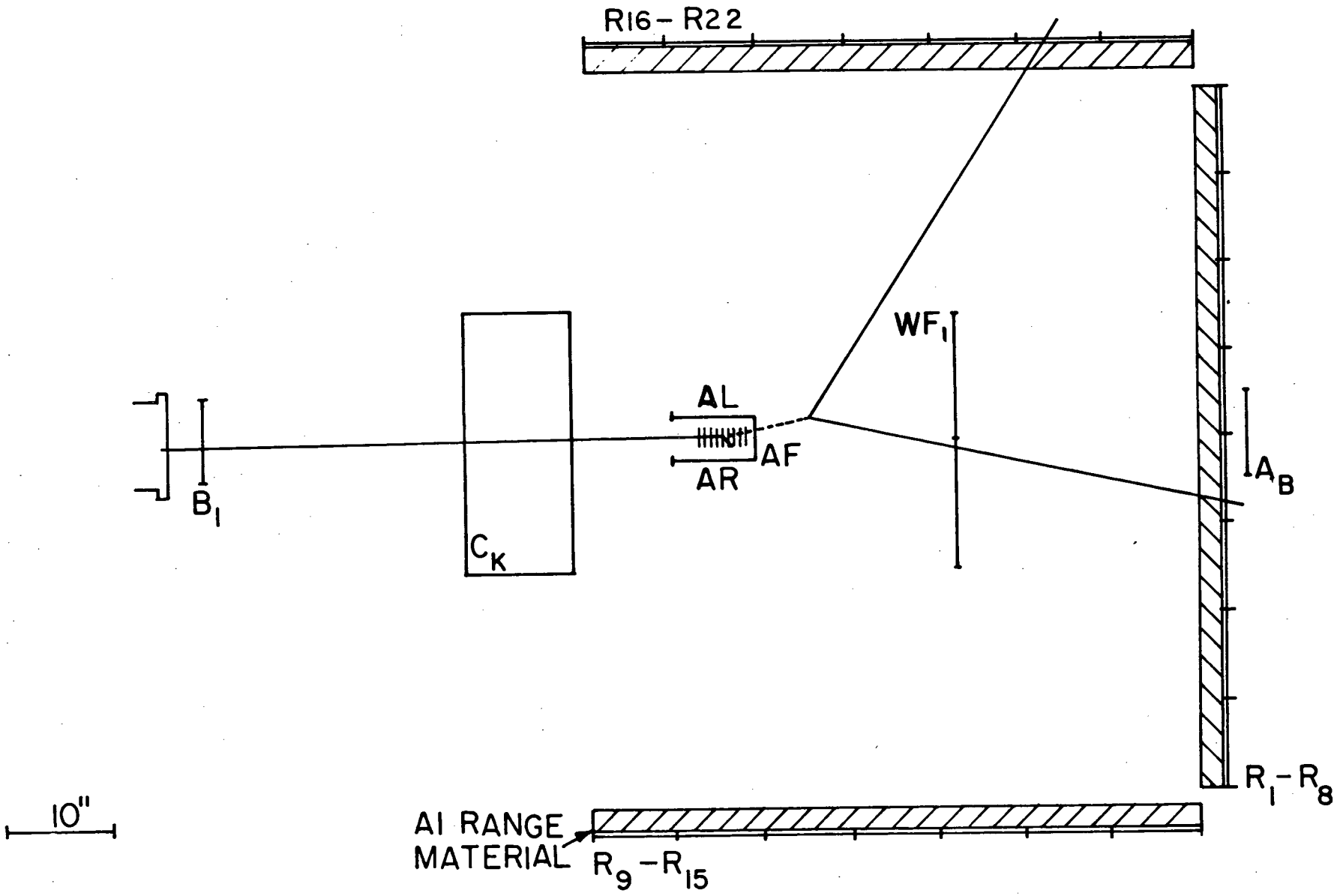
R16 – R22
WF1
AL
AF
AR
B1
CK
AB
R1 – R8
10"
Al RANGE MATERIAL
R9 – R15

the exit of the beam pipe and was intended to detect all charged particles in the beam. The Cherenkov counter C_K has been described elsewhere.[5,6] It was constructed so that a "positive" signal was given for kaons in the beam, and a veto signal was given for pions. The target counters, T1 through T10, indicated the target wafer in which the charge-exchange interaction occurred. In addition, each target counter was connected to a dual-pulse-height discriminator. The higher level discriminator was set to accept ~850 MeV/c protons. This criterion turned out to be equivalent to setting the discriminator so that the Landau tail of about 3% of the pions caused triggers. Surrounding the target area were anti-counters AL, AF, and AR, the function of which was to eliminate beam interaction events with energetic charged particles in the final state. R1 through R22 were hodoscope counters designed to detect two charged pions from neutral kaon decay. The purpose of counters WF_1 and WF_2 was to require a charged particle in the front quadrant. This requirement eliminated many triggers from kaon decay into $\pi^o\pi^o$, for example. Finally, A_B assisted in eliminating spurious events caused by beam particles. The dimensions of all of the counters are tabulated in Table 1.

b. Fast Electronics

The signals from the counters described above were detected and processed by the standard University of Illinois fast electronics logic modules.

An event of interest resulted in a fast coincidence of signals from B1, T1, C_K, WF_1 or WF_2, and any two of the R1 through R22 counters; furthermore, to qualify as a "master trigger," this fast coincidence had to occur with no signals from AL, AF, AR, A_B, or any three or more of the R1 through R22 counters. In short, the coincidence-anticoincidence requirement for a master trigger was written, in the standard notation, as

$$B1T1C_K(WF_1 \text{ or } WF_2)\overline{R^2(AL,AF,AR,R^3,A_B)}.$$

Table 1

Dimensions of Counters

Counter	Thickness (Inches)	Active Area ($Inches^2$)
B1	$\frac{1}{8}$	8X8
C_K	$\frac{3}{4}$	2X5
T1-T10	$\frac{1}{16}$	2X2
WF_1,WF_2	$\frac{1}{16}$	12X24
R1-R22	$\frac{1}{8}$	8X48
A_B	$\frac{1}{8}$	8X8
A_L	$\frac{1}{8}$	8X8
A_F	$\frac{1}{8}$	4.2X8
A_R	$\frac{1}{8}$	8X8

2. Range Material

Of course, not every master trigger was the result of a nice clean kaon charge-exchange and decay into $\pi^+\pi^-$. When a negative kaon beam was used, a potential source of master triggers was the interaction $K^-p \rightarrow \Lambda\pi^o$ with $\Lambda \rightarrow p\pi^-$.

Several methods were used to separate Λ production and decay events from kaon charge-exchange events. One method was the placement of two inches of aluminum in front of the R-counter hodoscope, as shown in Figure 3. This aluminum range material served to stop one or the other of the decay products of some fraction of the Λ decays, thus preventing the satisfaction of the master trigger requirements. The range material was particularly useful in preventing triggers from Λ decays where the opening angle between the proton and π^- would have been similar to an opening angle between two charged pions from $\overline{K}^o$ decay.

3. Targets

Six different materials--polyethylene, carbon, aluminum, copper, tin, and lead--were used as targets in this experiment. Nine wafers sandwiched between target counters T1 through T10 made up a target. Each of the wafers was 2" wide by $1\frac{3}{4}$" high. The measured density of each of the target materials is tabulated in Table 2. Also tabulated are the gm/cm^2 and the number of $atoms/cm^2$ presented to the beam by each of the target materials.

4. Event Tracking

The tracking of each event was accomplished with 15 dual-plane magnetostrictive wire spark chambers. The positions of all the chambers are shown in Figure 4. The dimensions of all the chambers are tabulated in Table 3.

The three small chambers in the beam, called Beam 1, Beam 2, and Beam 3, indicated the trajectory of the incoming charged particles which interacted in the target to produce a master trigger. Beam 2 chamber was at a 45^o angle with respect to the other two beam chambers.

Table 2

Targets

Target	Measured Density (gm/cm^3)	Measured $\frac{gm}{cm^2}$	$\frac{Atoms}{cm^2}$ ($\times 10^{23}$)
			CH_2-molecules/cm^2
Polyethylene	.946	6.78	2.901
Carbon	1.76	5.83	2.923
Aluminum	2.70	8.31	1.855
Copper	8.89	12.24	1.160
Tin	7.27	15.13	.7674
Lead	11.17	16.66	.4839

Figure 4. Top view of all the spark chambers

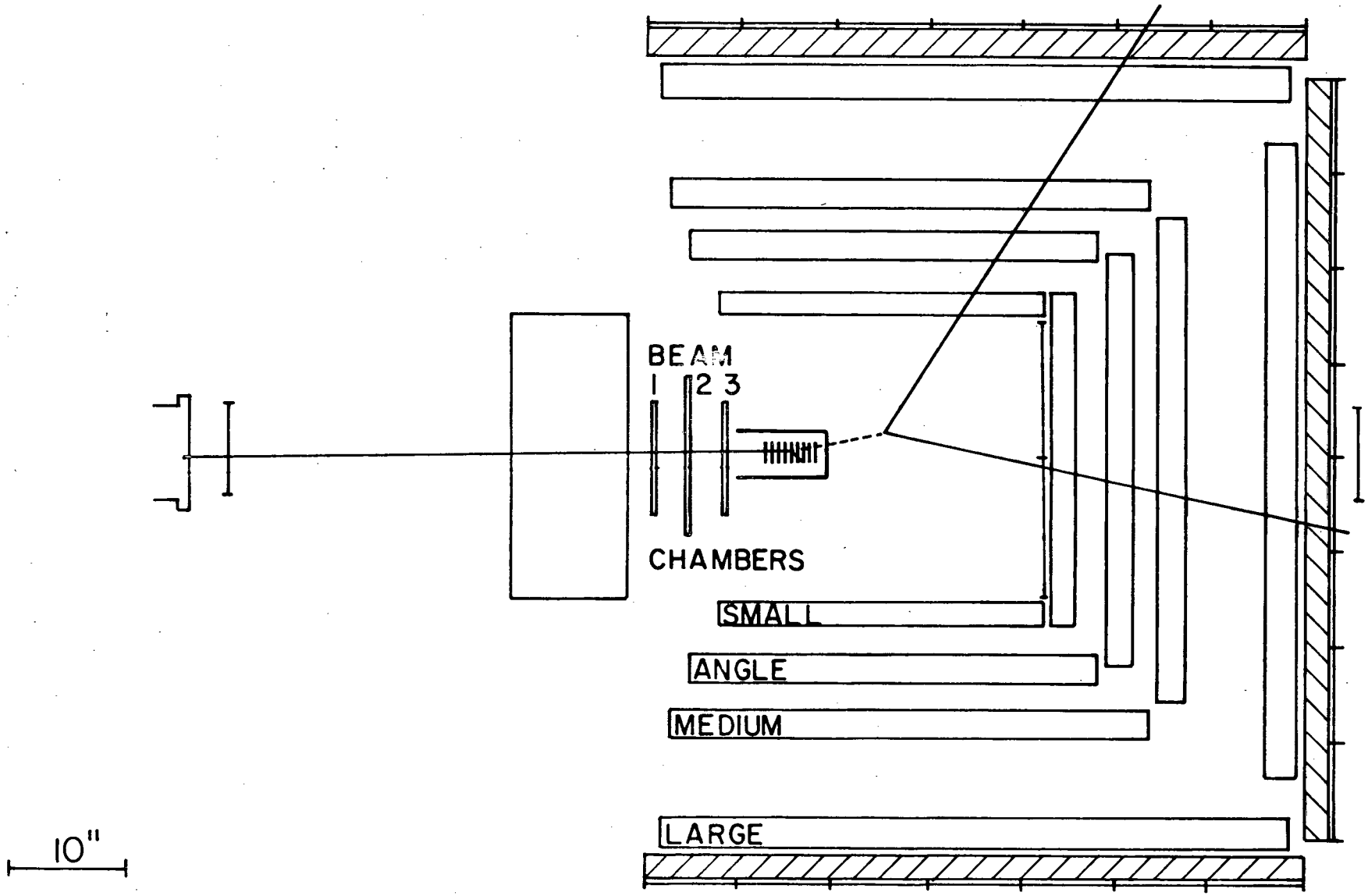
BEAM
1 2 3
CHAMBERS
SMALL
ANGLE
MEDIUM
LARGE
10"

Table 3

Spark Chamber Dimensions

Chambers	Overall Dimensions (in inches)	Active Dimensions (in inches)
Beam	$\frac{3}{8}$X10X10	$\frac{3}{8}$X6X6
Small	$2\frac{3}{4}$X28X28	$\frac{3}{8}$X24X24
Angle	$3\frac{1}{4}$X35X46	$\frac{3}{8}$X30X30
Medium	$3\frac{1}{4}$X41X41	$\frac{3}{8}$X36X36
Large	$3\frac{3}{4}$X54X54	$\frac{3}{8}$X48X48

The rest of the chambers, arranged in three quadrants around the target area, indicated the trajectories of any charged particles which had passed through them within approximately 500 ns prior to their being pulsed with high voltage. Within each quadrant, three of the chambers had two wire planes each, with the direction of the wires in one plane perpendicular to that of the wires in the other plane. Also in each quadrant there was one so-called "angle chamber." Each angle chamber had two wire planes, also. The wires in the two planes were oriented so that they made angles $\theta = \pm \arctan(.2)$ with respect to a horizontal plane.

The construction and operation of these chambers will be described in another thesis.[7]

5. Event Recording

a. Time Digitizing System

Sparks in the wire spark chambers along the paths of charged particles were detected by magnetostrictive wire ribbons in the usual manner.[8] Details of the construction and use of the magnetostrictive detection apparatus employed in this experiment are given in Appendix A. In addition to the sparks inside a given chamber, each chamber was equipped with so-called fiducial wires which were pulsed with high voltage each time the chamber was. The fiducial wires were positioned so that they defined a "window" between which real sparks from tracks in the chamber had to appear, if they were present at all.

The signals on the magnetostrictive ribbons from the fiducials and from real sparks in the chambers were detected, shaped, and amplified by Science Accessories Corporation Model 1001 preamplifiers, which were connected directly to Lecroy Research Systems Time Digitizers, Models 180 and 801. The time digitizers digitized the time intervals between the arrival of consecutive pulses from the magnetostrictive ribbons. In effect, the digitized intervals represented the coordinates in space of the sparks in the chambers.

b. Computer System

After each master trigger, the digitized information from the Lecroy system was read into the University of Illinois Xerox Data Systems Sigma 2 computer, under the control of RTAC*, a Real-Time Analysis Control program. The raw data from the Lecroy system was recorded on magnetic tape for every event. In addition the fiducial and spark coordinates and pulse height information from the target counters was analyzed by RECON**, an on-line reconstruction and analysis program. RECON reconstructed the tracks from each event that it had time to analyze and computed the values of a number of variables. Among the variables computed were these:

1) the position of interaction of the beam particle in the target;
2) the production angle of the neutral particle which later decayed to complete the master trigger;
3) the position of decay of that neutral particle;
4) the opening angle of the two charged decay products;
5) the angles between the direction of the decaying particle and the directions of each of the decay products;
6) the momentum of the decaying particle based on its production angle, assuming production on a single stationary nucleon;
7) the momentum of the decaying particle based on the opening angle of the decay products;
8) the difference between the momentum calculated in the two different ways for the decaying particle;
9) the coplanarity of the plane containing the two decaying particles and a plane containing the line between the production and decay points of the decaying particle.

*RTAC was written by R. Cullum.

**RECON was written by J. Frank.

All of the above quantities, and many others concerned primarily with monitoring the equipment, were stored in histograms which were updated on-line. The histograms could be displayed on an oscilloscope screen at will. At the end of each data run, approximately fifty histograms were checked visually by a physicist to determine whether all systems appeared to be working nominally. Particular attention was paid to any indications of inefficiency of a chamber or malfunction of a magnetostrictive pickup or time digitizer. Any histogram of particular concern or special interest was printed out using a teletype. All of the on-line histograms were zeroed before each run; however, prior to zeroing, the contents of some of the on-line histograms were transferred to locations in the computer where they were accumulated from one run to the next run of the same type. This procedure was useful, for example, in that it allowed a comparison of the number of K^o decays detected as a function of lifetime to that for $\overline{K}^o$ as the main experiment progressed.

Also, at the end of each run a "Run Summary" was printed out. The run summary contained information which indicated whether the spark chambers and the target counters and the Lecroy system were functioning normally. These run summaries were examined after each run by a physicist, and any indications of any malfunction in the previous run were given due attention. The run summary also told how many events had been examined by RECON during the previous run; and of those, it told how many, G, passed the front end of the apparatus satisfactorily. An event was counted in the total for G when there were no extra beam tracks, but there were enough sparks in the beam chambers to obtain the path of the incoming charged kaon; and the information from the target counters was sufficient to determine in which target wafer the interaction occurred. [The symbol G as defined above will be used in Treatment of the Data sections which follow.]

C. Treatment of the Data

During the experiment data was taken, alternately, with positive and negative kaon beams. For positive kaons, the charge-exchange production of K^o's was measured on carbon, aluminum, copper, tin, and lead targets. For negative kaons, both the charge-exchange production of $\overline{K}^o$'s and the production of Λ's was measured. In addition, polyethylene was used as a target for negative kaons, and cross sections were derived for $\overline{K}^o$ and Λ production from hydrogen.

Due to the relative simplicity of the K^+ studies, they will be described first.

1. K^+ Studies

For the K^+ target studies, a total of about 4.0×10^7 kaons were incident on the carbon target; 3.0×10^7, on the aluminum, copper, tin, and lead targets; and 2.0×10^7, on an "empty" target.

Before an interaction which resulted in a master trigger was identified as a charge-exchange and decay event, e.g.

$$K^+ + {}_Z N^A \rightarrow K^o + X$$
$$\qquad\qquad\quad \hookrightarrow \pi^+\pi^- \quad ,$$

the following conditions had to be satisfied:

1) Two tracks were reconstructed by RECON which "intersected" within the allowed decay volume; the distance of closest approach between the "intersecting" tracks was required to be $\leq .50"$. This requirement helped to eliminate the formation of "intersections" with random extra beam tracks.

2) The plane defined by the intersecting tracks was required to be coplanar with a plane containing the line from the K^o production point to the decay point to $\leq .31/D$ radians, where D was

the distance, in inches, from the production point to the decay point. This requirement reduced any 3-body background.*

3) The opening angle θ between the intersecting tracks was required to be $54^{o} \leq \theta \leq 100^{o}$.

4) The "half opening angles," that is, the angles between the direction of the decaying particle and each of the decay products, was required to be $> 13^{o}$.

5) The momentum as calculated from the K^{o} production angle was required to be within $\pm$ 200 MeV/c of the momentum as calculated from the opening angle between the intersecting tracks.

These same five conditions, or "cuts," were used for the identification of K^{-} charge-exchange and decay events. For the K^{-} interactions, conditions 3), 4) and 5) were particularly useful in separating $\Lambda \rightarrow p\pi^{-}$ events from $\overline{K}^{o} \rightarrow \pi^{+}\pi^{-}$ events. Of the Λ events detected, only about 7% had opening angles $> 54^{o}$, 2% had $\frac{1}{2}$-opening angles $> 13^{o}$, and $< 10\%$ satisfied condition 5). According to these estimates, only a very small fraction of the Λ's detected would be mistaken for $\overline{K}^{o}$'s.

It is important to realize that condition 5), on the momentum, and, to a lesser degree, condition 2), on the coplanarity, tended to select production events which occurred as a result of one and only one kaon-nucleon collision. Such an event is presumably kinematically and dynamically "hydrogen-like."

Events which were identified as K^{+} charge-exchange events according to the five criteria given above were accumulated in a number vs. lifetime

---

*The three-body background was already down by a factor of $\approx$500 compared to the two-body signal, just due to branching ratios.[11] Whatever three-body background may have remained was a negligible correction to the data for this experiment.

histogram. For the target studies described here, the total number of events N_{K^o} accumulated in that histogram for each run was the number of particular interest.

Also during each run the number of charged kaons focused on the target N_{K^+} and the number of master triggers M_1 were scaled on T.S.I. scalers, and at the end of each run the cumulative numbers were recorded.

A charge-exchange interaction and detection probability K_N was derived for each target material N:

$$K_N = \left[\frac{M_1}{N_{K^+}} \cdot \frac{N_{K^o}}{G}\right]_N - \left[\frac{M_1}{N_{K^+}} \cdot \frac{N_{K^o}}{G}\right]_{\text{TARGET EMPTY}}$$

with the symbols already defined above. (G was defined on p. 20.)

The cross section σ_N^K for charge-exchange on a nucleus, multiplied by an overall detection efficiency for kaons f^K, was then calculated for each target material:

$$f^K \sigma_N^K = \frac{K_N}{n}, \quad \text{(thin target approximation)},$$

where n was the number of nuclei/cm^2 which a target presented to the beam.

The detection efficiency f^K will be discussed and computed later in this thesis in the section under K^- studies. f^K is <u>assumed</u> to be independent of nuclear size. Under this assumption, charge-exchange cross sections for Al, Cu, Sn, and Pb <u>relative to that for C</u> were calculated, according to the formula

$$\frac{\sigma_N}{\sigma_C} = \frac{K_N/n_N}{K_C/n_C} .$$

The values for the relative cross sections and the data from which they were derived are tabulated in Table 4.

Table 4

Relative Cross Sections for K^o Production

Target	N_{K^+} ($\times 10^6$)	M_1	G	N_{K^o}	n ($\times 10^{23}$)	$f^K \sigma^K_N$ ($\times 10^{-29}$)	σ_N/σ_c
Empty	20.0	483	358	50			
Carbon	40.3	1872	1378	274	2.923	2.14 $\pm$ .15	1.0
Aluminum	30.0	1613	1280	287	1.855	4.8 $\pm$ .3	2.2 $\pm$ .2
Copper	30.19	1815	1414	297	1.160	8.0 $\pm$ .5	3.8 $\pm$ .3
Tin	30.15	1800	1384	301	.7674	12.7 $\pm$ .7	6.0 $\pm$ .5
Lead	30.0	1689	1321	317	.4839	19.9 $\pm$ 1.1	9.3 $\pm$ .8

2. K^- Studies

For the K^- target studies a total of about 5.6×10^7 kaons were incident on the polyethylene target, 6.2×10^7 on the carbon target; 1.6×10^7 on the aluminum, copper, tin, and lead targets; and 3.1×10^7 on an "empty" target.

The K^- studies were more involved than the K^+ studies because, in addition to charge-exchange production of $\bar{K}^o$'s, there was Λ production to consider. Furthermore, during the K^- studies the production of $\bar{K}^o$'s and Λ's from hydrogen was measured, and from this measurement, values of the overall detection efficiencies of the apparatus for the produced $\bar{K}^o$'s and Λ's were extracted.

a. Charge-Exchange on Complex Nuclei, Relative to Carbon

An interaction which resulted in a master trigger was identified as a charge-exchange and decay event, e.g.

$$K^- + {}_ZN^A \rightarrow \bar{K}^o + X$$
$$\qquad\qquad\quad \hookrightarrow \pi^+\pi^- \quad ,$$

when the criteria 1) through 5) of section II.C.1 were satisifed.

Charge-exchange cross sections for Al, Cu, Sn, and Pb, relative to that for C, were calculated in exactly the same way as described in section II.C.1. The results and the data from which they were calculated are tabulated in Table 5.

b. Charge-Exchange on Hydrogen

Measurement of the cross section for K^- charge-exchange on hydrogen was undertaken in this experiment primarily in order to provide a check on, and a measurement of, the operation and detection efficiencies of the experimental equipment; the hardware and the software. Two separate measurements of the K^- charge-exchange cross section on hydrogen were made. This cross section has been measured by others[12,13,14] and is known at 850 MeV/c incident momentum to an accuracy of better than 10%.[14]

Table 5

Relative Cross Sections for $\bar{K}^o$ Production

Target		N_{K^-} ($\times 10^6$)	M_1	G	$N_{\bar{K}^o}$	n ($\times 10^{23}$)	$f^K \sigma_N^K$ ($\times 10^{-24}$)	σ_N/σ_c
Empty	(1)	16.01	3180	2226	70			
	(2)	15.3	2785	2079	47			
CH_2	(1)	40.05	22693	18650	633	2.901	$f^K\sigma_H$ = 0.77±.06 (3)	σ_H/σ_c = 0.52±.05
	(2)	15.78	8348	6546	167			
Carbon	(1)	39.29	17998	14423	362	2.923	1.49±.10 (3)	1.0
	(2)	23.04	9803	7337	164			
Aluminum		16.00	6446	5259	80	1.855	1.08±.25	0.7 ±.2
Copper		16.45	5933	4692	84	1.160	2.0 ±.4	1.3 ±.3
Tin		16.00	5002	3984	91	.7674	3.9 ±.6	2.6 ±.5
Lead		15.79	4454	3349	70	.4839	3.6 ±1.0	2.4 ±.7

(1) High statistics measurement.

(2) Low statistics measurement.

(3) Average of (1) and (2). (with different detection efficiencies taken into account).

The charge-exchange cross section on hydrogen was derived in this experiment from sequential measurements taken with the carbon and the polyethylene targets.

The total thickness of the nine polyethylene target wafers was $2\frac{13}{16}$". This was as thick a target as could be sandwiched between the target counters T1 through T10. The total thickness of the nine carbon target wafers, 1.296", was chosen so that the carbon and the polyethylene targets each presented the same number of carbon atoms/cm^2 (to within <1%) to the K^- beam. Consequently, when the charge-exchange interaction and detection probability for carbon was subtracted from that for polyethylene, the remainder was the charge-exchange interaction and detection probability for hydrogen,

$$K_H = \left[\frac{M_1}{N_{K^-}} \cdot \frac{N_{\bar{K}^o}}{G}\right]_{CH_2} - \left[\frac{M_1}{N_{K^-}} \cdot \frac{N_{\bar{K}^o}}{G}\right]_{C} .$$

The two separate measurements of the K^- charge-exchange cross section on hydrogen were made with slightly different placements of the anti counters AL, AF, and AR. This resulted in a difference in detection efficiencies during the two measurements. The measurements were therefore considered separately. One of the measurements had three times more statistics on the polyethylene target and two times more statistics on the carbon target than the other measurement. The higher statistics measurements will be treated here first.

For the higher statistics measurement,

$$f^K \sigma_H^K = (1.32 \pm .09) \times 10^{-29} \text{ cm}^2.$$

The overall detection efficiency f^K is taken to be the product of two separable efficiencies ϵ^K_{DECAY} and $\epsilon^K_{APPARATUS}$: ϵ^K_{DECAY} is a factor which is dependent on

the placement of the anti counters AL, AF, and AR and on the branching ratio for $\bar{K}^o$ decay into π^+ and π^-; $\epsilon^K_{APPARATUS}$ is taken to be the overall efficiency, apart from ϵ^K_{DECAY}, of the apparatus for detection of the charge-exchange production of neutral kaons and their decay into π^+ and π^-.

The magnitude of ϵ^K_{DECAY} was determined by examination of an accumulated histogram of the number of $\bar{K}^o \rightarrow \pi^+\pi^-$ events vs. $\bar{K}^o$ lifetime. The histogram was accumulated for all of the runs with CH_2 and with C to determine the higher statistics charge-exchange cross section of hydrogen. See Figure 5. By taking the ratio of the area beneath the experimental points, A_E, to the area beneath a straight line (on a semi-log plot) with slope equal to $-(1/\tau_s)$ normalized to the experimental points in the 4-6 lifetime region, A_T, one obtains a measure of ϵ^K_{DECAY}:

$$\epsilon^K_{DECAY} = \frac{1}{2} \cdot \frac{2}{3} \cdot \frac{A_E}{A_T} ,$$

where the factor 1/2 represents the fraction of K^o_s in an initially pure $\bar{K}^o$ beam, and the factor 2/3 represents the branching ratio for K^o_s decay to π^+ and π^-.

For the higher statistics measurement

$$\epsilon^K_{DECAY,1} \simeq .042 .$$

The factor $\epsilon^K_{APPARATUS}$ was estimated early in the planning stages of this experiment to be[1/]

$$\epsilon^K_{APPARATUS} \simeq .08 .$$

Consequently,

$$f^K \simeq (.042)(.08) = 3.36\times10^{-3} \qquad \text{(for higher statistics data)}$$

and

$$\sigma_H{}^K = \frac{(1.32\pm.09)\times10^{-29}\ cm^2}{f^K}$$

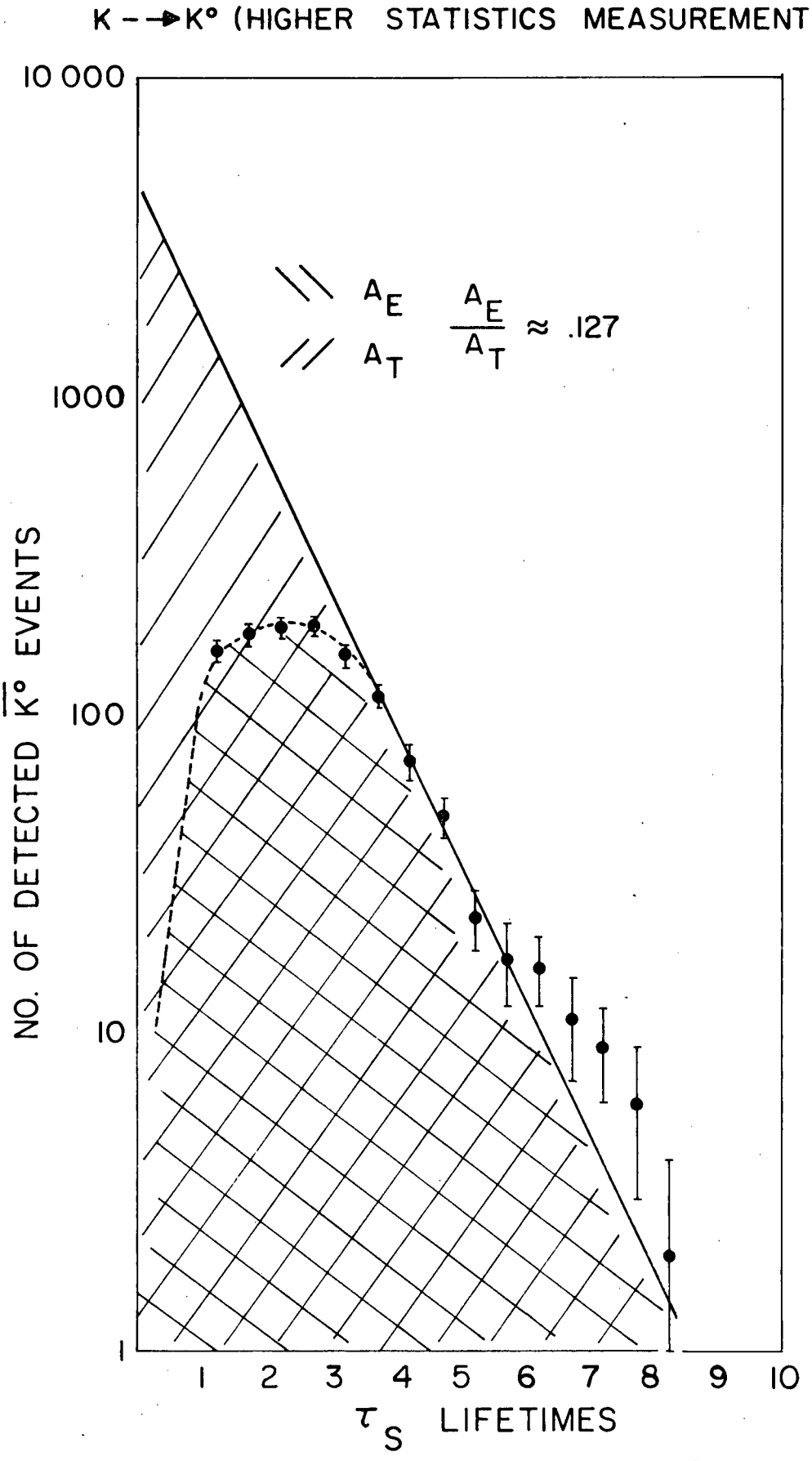
K − → K° (HIGHER STATISTICS MEASUREMENT
10 000
1000
100
10
1
NO. OF DETECTED $\overline{K}°$ EVENTS
A_E
A_T
$\frac{A_E}{A_T} \approx .127$
1 2 3 4 5 6 7 8 9 10
τ_S LIFETIMES

$$\sigma_H^K \simeq (3.9\pm.3)\text{mb} ,$$

where the error shown is only the statistical standard deviation.

The value of the cross section on protons for 850 MeV/c K^- charge-exchange that is quoted in the literature[14] is $(4.0\pm.3)$mb. The experimental value determined above agrees well with the "known" value of the cross section.

Working backwards, the "known" value of the cross section can be used to obtain an experimental value for $\epsilon^K_{APPARATUS}$ and its uncertainty:

$$f^K = \epsilon^K_{DECAY}\,\epsilon^K_{APPARATUS} = \frac{(1.32\pm.09)\times10^{-29}\ \text{cm}^2}{(4.0\pm.3)\times10^{-27}\ \text{cm}^2}$$

$$= (3.3\pm.3)\times10^{-3}$$

$$\epsilon^K_{APPARATUS} = \frac{(3.3\pm.3)\times10^{-3}}{\epsilon^K_{DECAY}}$$

$$\simeq \frac{(3.3\pm.3)\times10^{-3}}{.042} = (7.9\pm.7)\times10^{-2} ,$$

where the error quoted includes the uncertainty in the "known" value of the cross section and the statistical standard deviation in the value measured for $f^K\,\sigma_H^K$.

Now, for the lower statistics measurement of the cross section, ϵ^K_{DECAY} had a different value than determined above. Determined in the same way as described above, its value for the lower statistics measurement was

$$\epsilon^K_{DECAY} \simeq \frac{1}{2}\cdot\frac{2}{3}\cdot(.080) .$$

Using this value for ϵ^K_{DECAY} and the value of $\epsilon^K_{APPARATUS}$ determined above, the value of the overall detection efficiency during the lower statistics measurement can be determined:

$$f^K \simeq \frac{1}{3}(.080)(7.9\pm.7)\times10^{-2}$$

$$f^K \simeq (2.1\pm.2)\times10^{-3} \qquad \text{(for lower statistics data)} .$$

This value for f^K will be used in later sections of this thesis to calculate $K^{\pm}$ charge-exchange cross sections on complex nuclei.

It is important to note that the value derived above for f^K does not take into account the fact that for K^+ charge-exchange a proton is produced together with a neutral kaon; and the proton will in some cases pass through the anti-counters, causing the event to be vetoed. Only crude measurements were made of the effect of such proton vetoes. These indicated that f^K for K^+ charge-exchange could be ~35% smaller than stated above.

c. Lambda Production from Hydrogen

In this experiment, whenever a K^- beam was incident on the target, a large number of lambda hyperons were detected, since the production of a Λ and its subsequent decay into p and π^- often satisfied all the master trigger requirements described in section II.A.3.a. A K^- interaction which resulted in a master trigger was identified as a "Λ event," e.g. $K^- + {}_Z N^A \rightarrow \Lambda + X$ (with $\Lambda \rightarrow p+\pi$), if the following conditions were satisfied:

1) and 2) Intersection and coplanarity conditions. These were the same as conditions 1) and 2) in section II.B.1.

3) The opening angle θ between the intersecting tracks was required to be $\theta < 54^\circ$; or, if $\theta > 54^\circ$, the angle that one of the tracks made with respect to the Λ direction had to be $\leq 13^\circ$.

Two separate measurements of the cross section σ_H^{Λ} for K^- lambda production on hydrogen were made, one with higher statistics than the other. The Λ production measurements were done concurrently with the K^- charge-exchange measurements. The procedure for extracting the cross section for lambda production from hydrogen from the measurements taken with the carbon and the polyethylene targets was the same as has already been described for

the charge-exchange case, except, of course, in this case the total number of events N_Λ accumulated in a histogram of the number of Λ events vs lifetime was the number of particular interest.

The Λ production and detection probably, L, from hydrogen was given by

$$L_H = \left[\frac{M_1}{N_{K^-}} \cdot \frac{N_\Lambda}{G}\right]_{CH_2} - \left[\frac{M_1}{N_{K^-}} \cdot \frac{N_\Lambda}{G}\right]_C ,$$

The Λ production cross section on hydrogen, multiplied by an overall detection efficiency for Λ's, f^Λ, was given by $f^\Lambda \sigma^\Lambda = L_H/n_H$, where n_H was the number of hydrogen nuclei/cm^2 that the polyethylene target presented to the beam. Due to slightly different placements of the anti-counters AL, AF, and AR during the two separate measurements, f^Λ for the higher statistics measurement was slightly different from f^Λ for the lower statistics measurement.

Following the procedure that was already described in the $\overline{K}^o$ case, f^Λ can be calculated for both the high statistics and the low statistics measurements of lambda production from hydrogen. For the higher statistics measurement, $f^\Lambda \sigma_H{}^\Lambda$ was measured to be

$$f^\Lambda \sigma_H{}^\Lambda = (.0748 \pm .0048) \times 10^{-27} .$$

From the literature[14]

$$\sigma_H{}^\Lambda = (2.7 \pm .2)\text{mb}.$$

Therefore

$$f^\Lambda = (2.77 \pm .27) \times 10^{-2} \qquad \text{(for higher statistics data)}$$

$$f^\Lambda = \epsilon^\Lambda_{DECAY} \; \epsilon^\Lambda_{APPARATUS} .$$

For the higher statistics measurement ϵ^Λ_{DECAY}, determined just as was described

above for ϵ^{K}_{DECAY}, was found to be

$$\epsilon^{\Lambda}_{DECAY,1} \approx \frac{2}{3}(.42) \ .$$

Thus,

$$\epsilon^{\Lambda}_{APPARATUS} \approx (10.0\pm1.0)\times10^{-2} \ .$$

Then, for the lower statistics data, for which

$$\epsilon^{\Lambda}_{DECAY,2} \approx \frac{2}{3}(.36) \ ,$$

the value of f^{Λ} is

$$f^{\Lambda} = (2.4\pm.2)\times10^{-2} \quad \text{(for lower statistics data).}$$

This value for f^{Λ} will be used in a later section of this thesis to calculate Λ production cross sections from K^- incident on complex nuclei.

d. Lambda Production from Complex Nuclei, Relative to Carbon

The values of

$$n f^{\Lambda}\sigma_N{}^{\Lambda} = L_N = \left[\frac{M_1}{N_{K^-}} \cdot \frac{N_\Lambda}{G}\right]_N - \left[\frac{M_1}{N_{K^-}} \cdot \frac{N_\Lambda}{G}\right]_{\text{TARGET EMPTY}}$$

were computed for the carbon, aluminum, copper, tin, and lead targets. The values of $f^{\Lambda}\sigma_N{}^{\Lambda}$, the cross sections for lambda production, relative to carbon, and the data from which the results were computed are tabulated in Table 6.

3. Comparison of Relative Cross Sections

It is interesting to compare the K^+ and K^- charge-exchange and Λ production cross sections on complex nuclei, relative to carbon. The relative cross sections tabulated in Tables 4, 5, and 6 are plotted in Figure 6, vs $A^{2/3}$, where A is the mass number of the complex nuclear targets used.

The striking feature to be noticed in Figure 6 is the relatively steep and apparently linear increase in the K^+ charge-exchange cross section

Table 6

Relative Cross Sections for Λ Production

Target	N_{K^-} ($\times 10^6$)	M_1	G	N_Λ	n ($\times 10^{23}$)	$f^\Lambda \sigma_N^\Lambda$ ($\times 10^{-27}$)	σ_N/σ_C
Empty (1)	16.01	3180	2226	1089			
Empty (2)	15.3	2785	2079	929			
CH_2 (1)	40.05	22693	18650	9145	2.901	$f^\Lambda \sigma_H$ = .077±.004 (3)	σ_H/σ_C = .20±.01
CH_2 (2)	15.78	8348	6546	3113			
Carbon (1)	39.29	17998	14423	7352	2.923	.377±.006 (3)	1.0
Carbon (2)	23.04	9803	7337	3387			
Aluminum	16.00	6446	5259	2418	1.855	.56 ±.02	1.49±.05
Copper	16.45	5933	4692	2254	1.160	.79 ±.03	2.10±.08
Tin	16.00	5002	3984	1890	.7674	.88 ±.04	2.3 ±.1
Lead	15.79	4454	3349	1554	.4839	1.03 ±.06	2.7 ±.2

(1) High statistics measurement.

(2) Low statistics measurement.

(3) Average of (1) and (2), (with different detection efficiencies taken into account).

Figure 6. Cross sections on Al, Cu, Sn, and Pb relative to C for K^+ and K^- charge-exchange and Λ production from K^-.

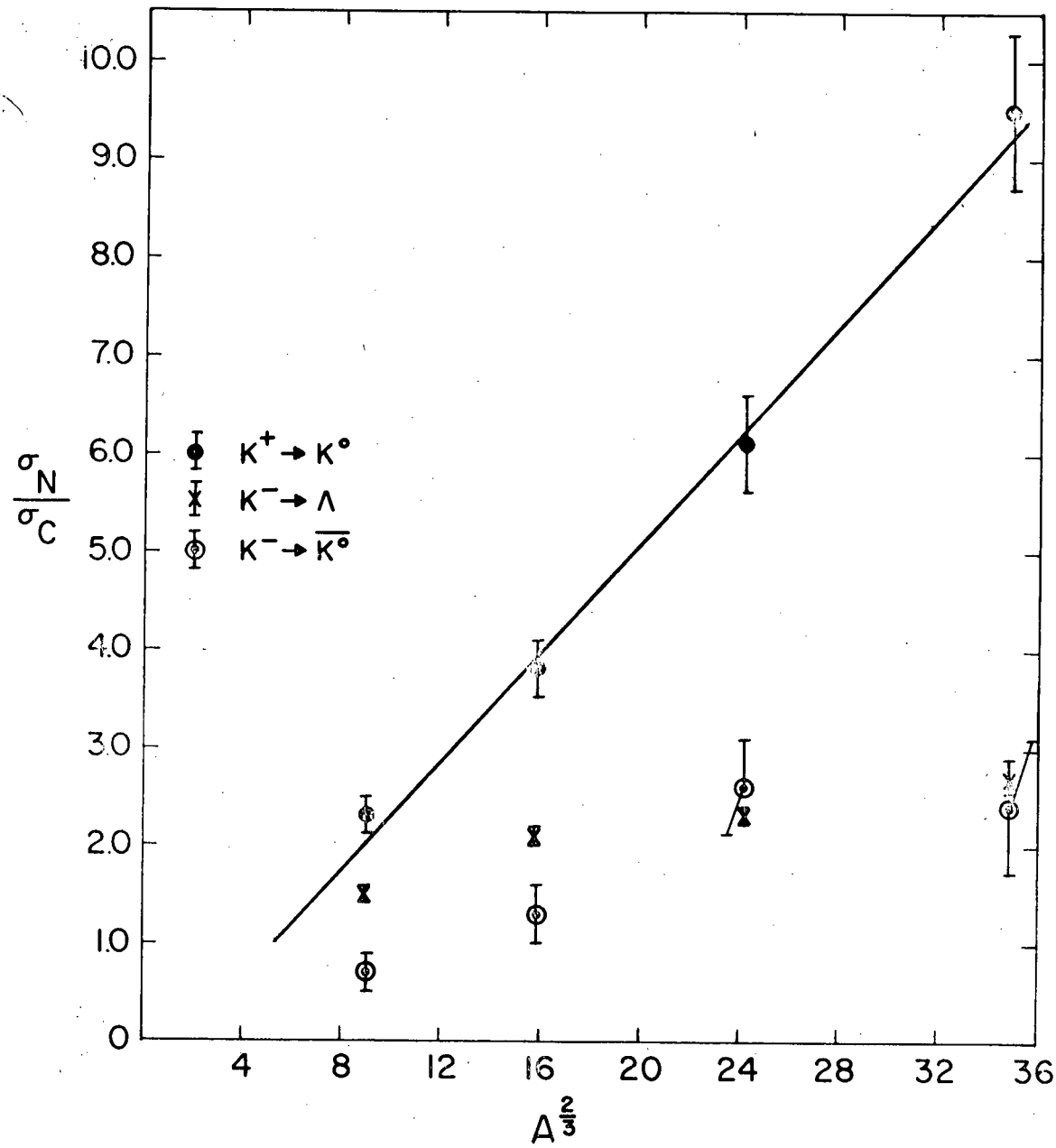
10.0
9.0
8.0
7.0
6.0
5.0
4.0
3.0
2.0
1.0
0
$\frac{\sigma_N}{\sigma_C}$
$K^+ \rightarrow K^\circ$
$K^- \rightarrow \Lambda$
$K^- \rightarrow \overline{K^\circ}$
4
8
12
16
20
24
28
32
36
$A^{\frac{2}{3}}$

as $A^{2/3}$ increases. This, in contrast to the very small dependence on A of the K^- charge-exchange and Λ production cross sections.

Qualitatively, the explanation of this result is a consequence of available reaction channels and the conservation of hypercharge in strong interactions. For kaons, hypercharge equals strangeness. In the case of K^+'s incident at 850 MeV/c on nuclei, the only strong interaction channels of significance that are energetically allowed are elastic scattering and charge-exchange.[15] The S = +1 K^+ must come out of the target either as a K^+ or an S = +1 K^o. In contrast, K^-'s incident at 850 MeV/c on nuclei have several alternate interaction channels energetically available.[16] The S = -1 K^- can interact with protons or neutrons to produce Λ's and Σ^o's, and also $\Sigma^\pm$'s, in addition to charge-exchanging to produce $\bar{K}^o$'s. The distribution of the S = -1 quantum number among the various available final states evidently results in a much slower increase with A in the cross section for a given K^- interaction channel than the K^+ charge-exchange results would naively lead one to expect.

4. Absolute Cross Sections on Complex Nuclei

In this section, absolute cross sections for $K^\pm$ charge-exchange and Λ production are presented, and then a discussion of results and models follows. As will be seen in the Monte Carlo section, III, the values obtained are dependent on experimental cuts that are A-dependent.

a. K^+ Results

Again, the K^+ results are presented first. The mean values of the cross sections are obtained by dividing the mean values of $f^K\sigma_N{}^K$ in Table 4 by the mean value of $f^K = (2.1\pm.2)\times10^{-3}$ which was determined in section II.C.2.b . The cross sections are plotted in Figure 7. The error bars in Figure 7 represent the root-mean-square of the statistical errors on the values of $f^K\sigma_N{}^K$ and the statistical and experimental errors on the value derived for f^K.

Figure 7. Cross sections for K^+ charge-exchange, plotted versus $A^{2/3}$.

(The results presented in Figs. 7-10 were calculated with the assumption that any momentum and angular dependence of the experimental efficiencies of sections II.C.2., b. and c., did not affect the A-dependence of the cross sections.)

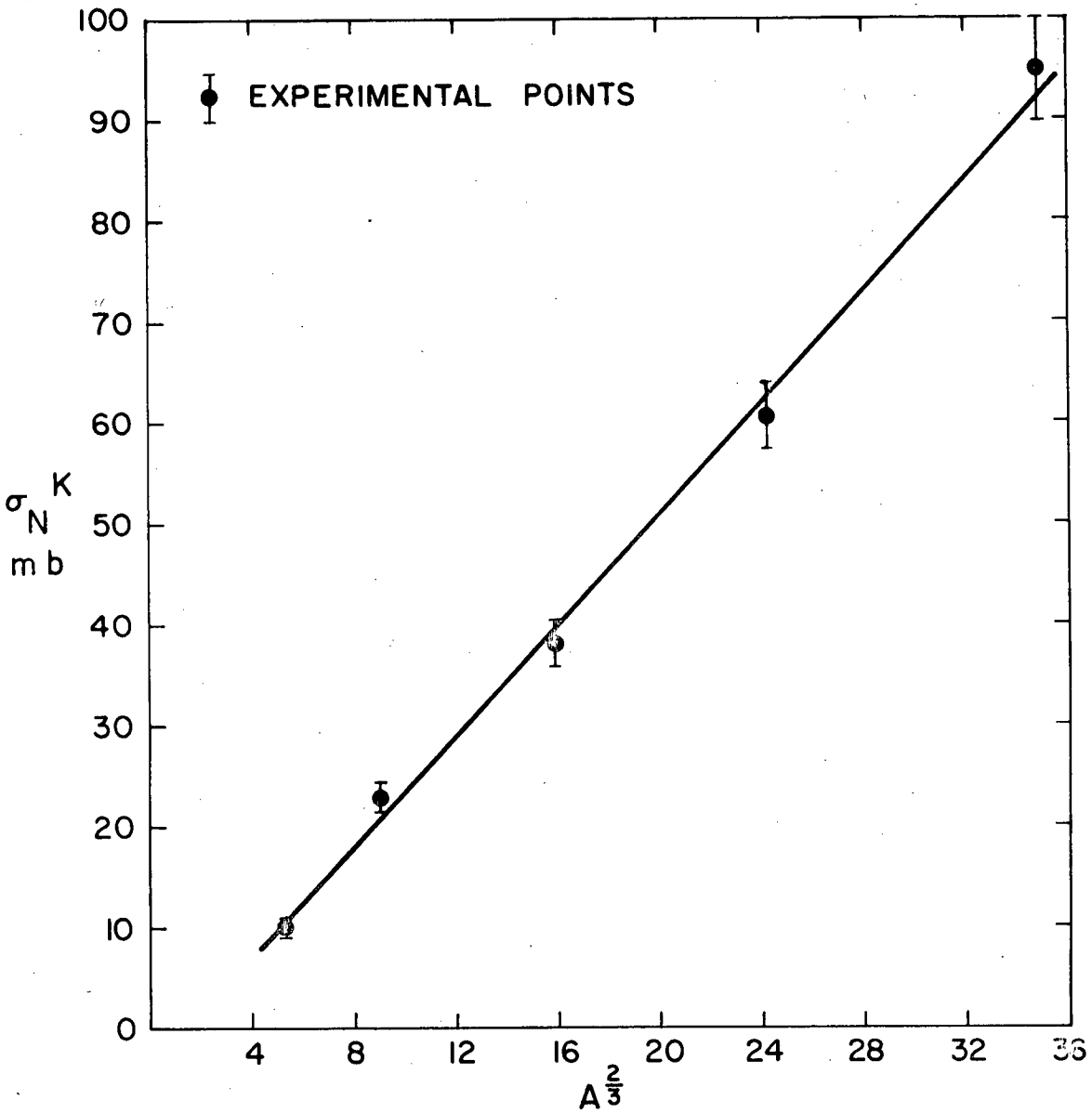
EXPERIMENTAL POINTS
σ_N^K
m b
100
90
80
70
60
50
40
30
20
10
0
4
8
12
16
20
24
28
32
36
$A^{\frac{2}{3}}$

The abscissa in Figure 7 is $A^{2/3}$, and the straight line is a least-squares fit to the data, with slope=(2.74±.12)mb and intercept=(-3.8±1.3)mb. χ^2 for this fit equals 3.6, and for three degrees of freedom results in a confidence level of .31. On a χ^2-basis alone, this fit is quite acceptable.

However, another aspect must be considered. Plotting the data vs. $A^{2/3}$ implicitly assumes a model for the cross sections, such as $\sigma_N^K = \pi(r_o A^{1/3})^2 + \text{const.}$, where r_o is a nuclear unit radius. Upon assuming such a model, the value of r_o is determined from the slope of the straight-line fit to the data. In the case presented in Figure 7, the result is $r_o = (.295 \pm .006)$fm. This value is far different from the expected value,[17] ~1.3 fm.

Consequently, another model which was used by others to fit data for Λ production from negative pions incident on complex nuclei[20] was tried. In this model the data are plotted versus $(\frac{A-Z}{A})A^{1/3}$. The fit is displayed in Figure 8. An acceptable confidence level equal to .11 results from $\chi^2 = 6.1$ for 3 degrees of freedom. The full expression for the cross section is $\sigma_N^K = 2\pi r_o A^{1/3} \delta(\frac{A-Z}{A}) + \text{const.}$: The cross section for hydrogen-like charge-exchange production of K^o's from complex nuclei is given essentially by the area $2\pi r_o A^{1/3}\delta$, of a narrow rim around the edge of a spherical nucleus, multiplied by the fraction $(\frac{A-Z}{A})$ of collisions which occur with neutrons. δ is the "effective rim width" and is assumed to be independent of Z or A.

The least-squares-fitted straight line in Figure 8 has slope = (31.2±1.4)mb and intercept = (-26.1±2.2)mb. Assuming r_o = 1.3fm,[18] the value for δ is (.38±.02)fm. This value for δ will be compared to values found from Λ production and K^- charge-exchange in succeeding sections of this thesis.

b. K^- Results

The K^- results will be presented in two subsections, one on Λ production and one on K^o production.

Figure 8. Cross sections for K^+ charge-exchange, plotted versus $(\frac{A-Z}{A})A^{1/3}$.

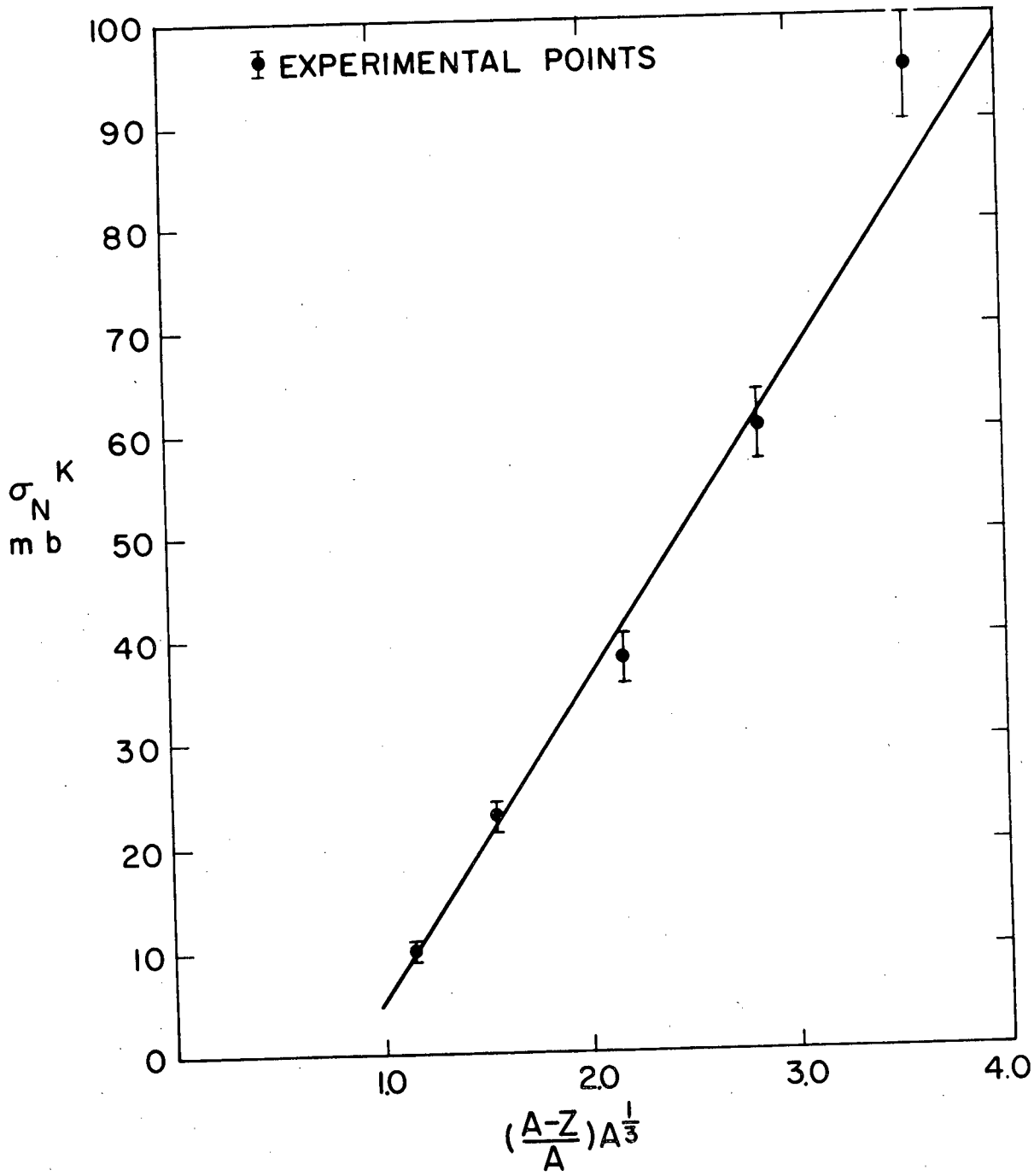
EXPERIMENTAL POINTS
100
90
80
70
60
50
40
30
20
10
0
σ_N^K
m b
1.0
2.0
3.0
4.0
$(\frac{A-Z}{A})A^{\frac{1}{3}}$

i. Λ Production

The mean values of the cross sections and their error bars were calculated as described in the previous section for K^+ Results, except that the values of $f^{\Lambda}\sigma_N^{\Lambda}$ were taken from Table 6, and the value of $f^{\Lambda} = (2.4\pm.2)\times10^{-2}$ was that derived in section II.C.2.c.

The cross sections are plotted versus $A^{1/3}$ in Figure 9. Also shown is a straight line fitted by least-squares to the data. Its slope = (9.39±.20)mb; intercept = (-6.1±.3)mb. With $\chi^2 = 16.0$ and 4 degrees of freedom, the straight line fits the data with a confidence level of .0035.

The model leading to this particular choice for the abscissa is similar to the second one described in the section on K^+ Results, except that the cross section for hydrogen-like production of Λ's from K^-'s on neutrons was taken to be equal to that on protons.[16] Symbolically,

$$\sigma_N^{\Lambda} = (\frac{Z}{A})2\pi r_o A^{1/3}\delta + (\frac{A-Z}{A})2\pi r_o A^{1/3}\delta + \text{const.}$$

$$= 2\pi r_o A^{1/3}\delta + \text{const.}$$

Again r_o was taken to be 1.3 fm,[19] and from the slope of the straight line in Figure 9, the effective rim width δ = (.115±.002)fm was computed.

ii. K^- Charge-Exchange

The mean values of the cross sections and their error bars for K^- charge-exchange were calculated in the same way as has already been described for K^+ charge-exchange. The values of $f^K\sigma_N^K$ were taken from Table 5.

Figure 10 shows the cross sections plotted versus $\frac{Z}{A}A^{1/3}$, and a straight line has been fitted by least-squares to the data, with slope (8.9±1.3)mb and intercept = (-4.8±1.5)mb. The χ^2 confidence level for this fit is $<10^{-4}$!

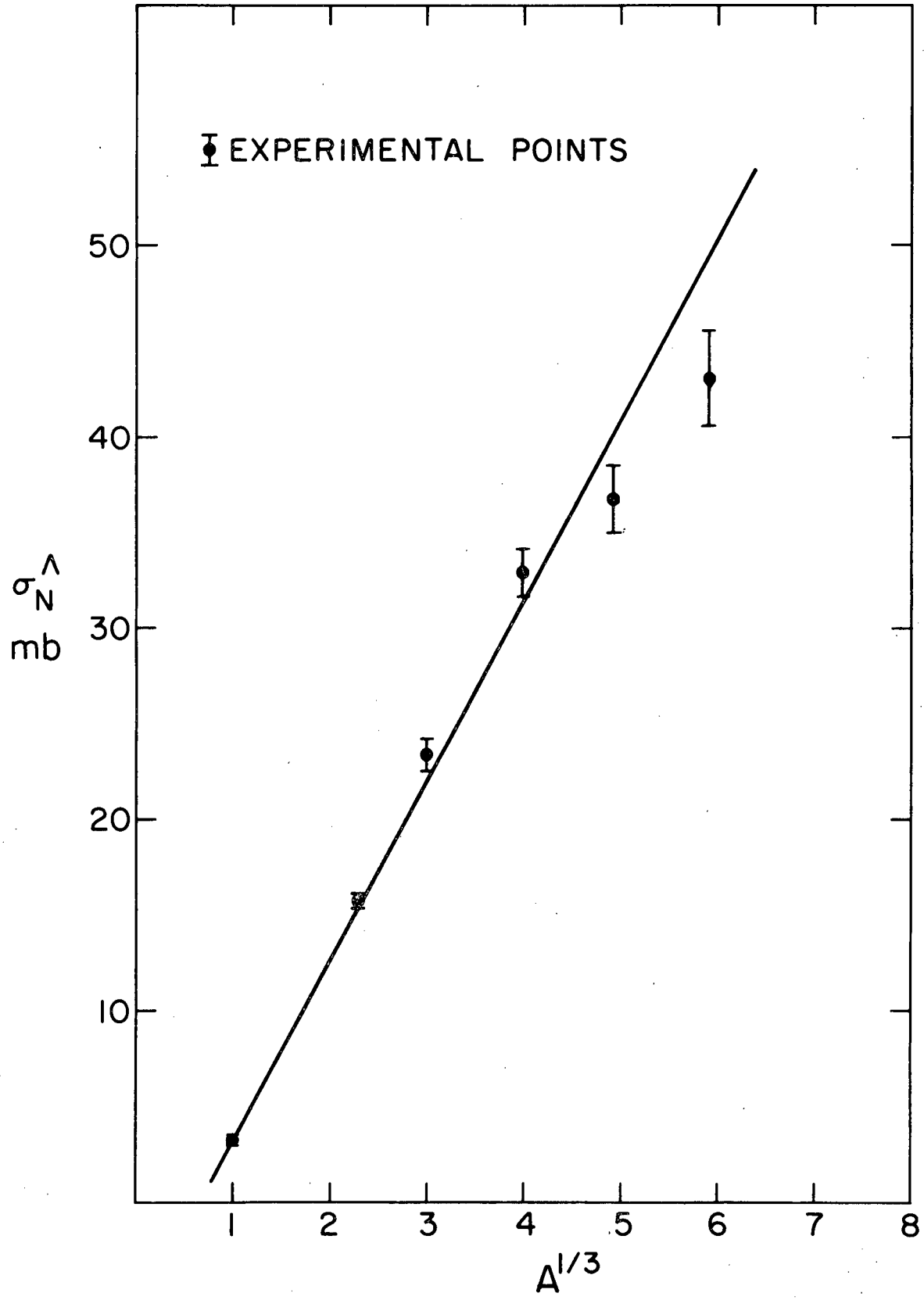
EXPERIMENTAL POINTS
50
40
30
20
10
σ_N^{Λ}
mb
1
2
3
4
5
6
7
8
$A^{1/3}$

Figure 10. Cross sections for K^- charge-exchange, plotted versus $(\frac{Z}{A})\ A^{1/3}$.

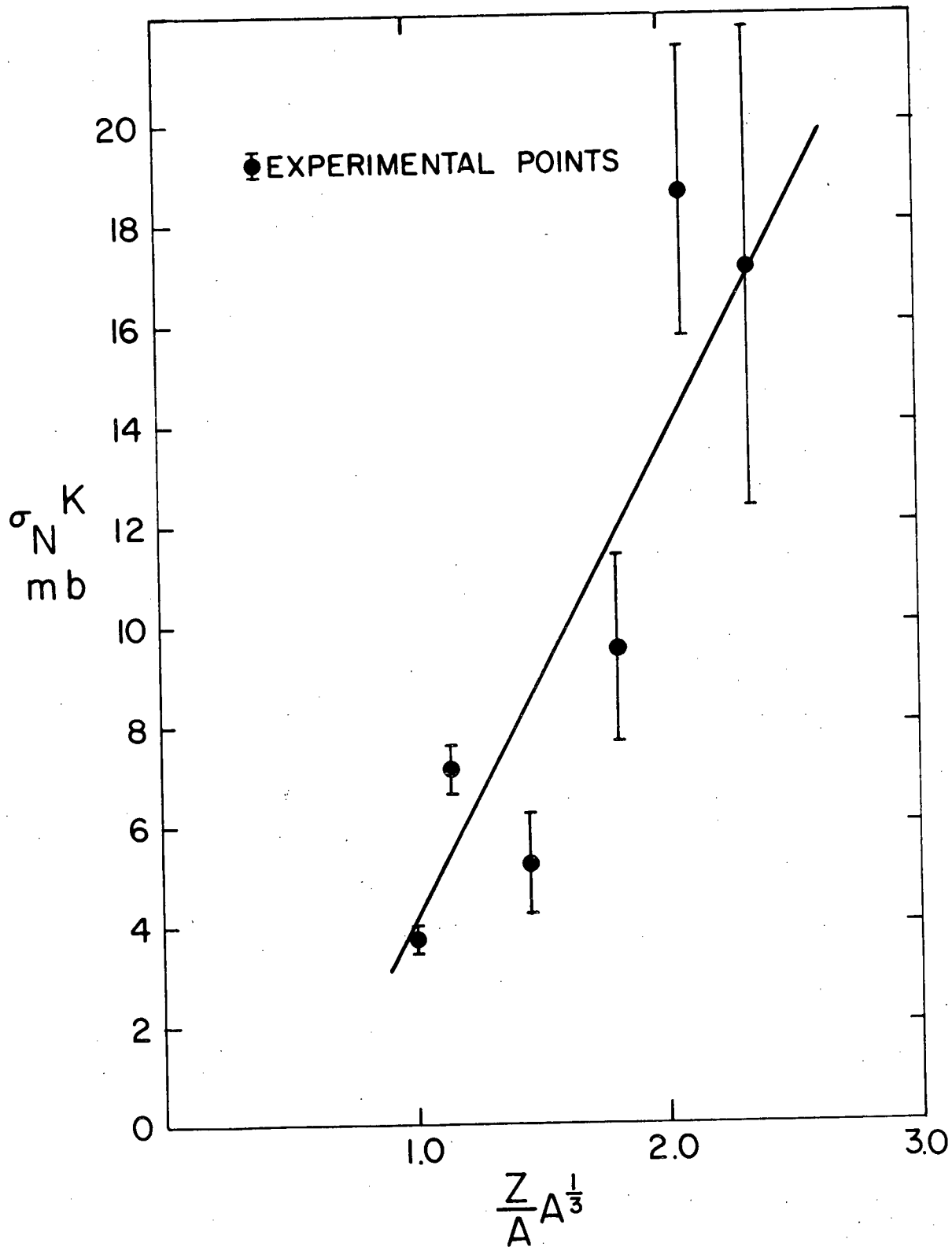
EXPERIMENTAL POINTS
σ_N^K mb
20
18
16
14
12
10
8
6
4
2
0
1.0
2.0
3.0
$\frac{Z}{A}A^{\frac{1}{3}}$

The hypothesis leading to this particular choice of $A^{1/3}$ dependence was the same as the second one described for K^+ charge-exchange, except in this case the fraction of collisions that occur with protons is substituted for that with neutrons. Symbolically,

$$Z\sigma_A^K = \left(\frac{Z}{A}\right) 2\pi r_o A^{1/3}\delta + \text{const.}$$

Again, with $r_o = 1.3$ fm, the slope of the line gives

$$\delta = (.11 \pm .02)\text{fm}.$$

c. Comparison and Discussion

The "effective rim width" model used in the preceding sections for the hydrogen-like production of K^o's, Λ's, and $\overline{K}^o$'s has been proposed previously by Frankel, et al.,[20] who found a good linear fit to cross sections for Λ production from π^- interactions in nuclei when the data were plotted versus $\left(\frac{Z}{A}\right)A^{1/3}$. In their case, a value was extracted for $\delta = .25$ fm. (No error was quoted! Nor was it clear what value was used for r_o.)

δ represents an "effective rim width" for the hydrogen-like production in nuclei of particles which are eventually detected in a coincidence-type experiment. In this spirit of this model, one expects to detect only the fraction of the particles of interest that are produced on nucleons at the periphery of a nucleus, so that the incoming charged kaons or the product particles have small probability for multiple strong interactions with the remaining nucleons.

It seems reasonable that the effective rim width should be dependent on partial production cross sections and on the mean free paths (m.f.p.) of the incident and product particles in nuclear matter. Qualitatively, such a dependence could account for the significant difference between $\delta = (.38 \pm .02)$fm for K^o's produced from K^+'s with m.f.p. ~ 6.6 fm and the δ's for $\overline{K}^o$'s and

Λ's, (.11$\pm$.02)fm and (.115$\pm$.002)fm, respectively, produced from K^-'s with m.f.p. $\sim$ 2.2 fm.

In reference 20, lambdas were produced from 1055 MeV/c π^-'s with m.f.p. $\approx$ 1.6 fm incident on complex nuclei. The reactions were $\pi^- + p \rightarrow \Lambda + K^o$, $\sigma_{\Lambda K} \approx .57$ mb, and $\pi^- + p \rightarrow \Sigma^o + K$, $\Sigma^o \rightarrow \Lambda + \gamma$, $\sigma_{\Sigma K} \approx .35$ mb. It is not evident how to account even qualitatively for the fact that the δ for Λ production found in reference 20 was larger than that found in the experiment for this thesis.

Apart from the preceding qualitative speculations, more quantitative tests of the data were applied. The production cross sections were plotted against a variety of different dependences on the power of A. These are indicated in the top line of Table 7. In each case, straight lines were fitted to the data by least-squares, and values of χ^2 were computed. The values of χ^2 and the corresponding confidence levels are tabulated in Table 7.

In the K^o case, plots of the data versus an $A^{1/3}$- or an $A^{2/3}$-type dependence appear to give good fits, with acceptable χ^2 confidence levels. In order to determine a preference for one type dependence or the other, one can resort to the values of the parameters associated with models, as done in section II.4.a. Possible models behind the different abscissas of Table 7 are indicated in the top line of Table 8. As pointed out in section II.4.a, the $A^{2/3}$ models result in values of r_o which seem unreasonably* small, while the $A^{1/3}$ model results in a value for δ which is reasonable.

---

*It may reasonably be argued that the values computed for r_o should be multiplied by a factor that takes into account the ratio of the number of K^o's produced to the total number of K^+ interactions. In the $K^+ \rightarrow K^o$ case, one estimate of the factor could be $[((A-Z)/A)(\sigma(K^+n \rightarrow K^o p)/\sigma(K^+n \rightarrow all))]^{-\frac{1}{2}} \approx [(.5)(.475)]^{-\frac{1}{2}} \approx 2$. Even when multiplied by this factor the values of r_o remain less than 1 fm.

Table 7

Abscissa		(A-Z)	$A^{2/3}$	$\frac{A-Z}{A}\cdot A^{1/3}$	$\frac{A-Z}{A}\cdot A^{2/3}$	$A^{1/3}$	A	Z	$\frac{Z}{A}\cdot A^{1/3}$	$\frac{Z}{A}\cdot A^{2/3}$
K^o 3 Degrees of Freedom	χ^2 = C.L.* =	21.1 1.3×10^{-4}	3.6 .31	6.1 .11	5.1 .16					
Λ 4 Degrees of Freedom	χ^2 = C.L. =		269. $< 10^{-4}$			16.0 .0035	739. $< 10^{-4}$	641. $< 10^{-4}$	325. $< 10^{-4}$	253. $< 10^{-4}$
$\overline{K}^o$ 4 Degrees of Freedom	χ^2 = C.L. =	14.9 .005						21.0 3.5×10^{-4}	26.3 $< 10^{-4}$	16.8 .0025

*C.L. = χ^2 confidence level.

Table 8

Model for σ_N	$\sigma(K_n^+ \to K_p^o)$ (A-Z)	$\pi r_o^2 A^{2/3}$	(1) $2\pi r_o A^{1/3}\delta$ $(\frac{A-Z}{A})$	$(\frac{A-Z}{A})$ $\pi r_o^2 A^{2/3}$	(1) $\pi r_o A^{1/3}\delta$	$\sigma(K^- N \to \Lambda X)$ A	$\sigma(K_p^- \to \overline{K}^o n)$ Z	(1) $2\pi r_o A^{1/3}\delta$ $(\frac{Z}{A})$	$(\frac{Z}{A})$ $\pi r_o^2 A^{2/3}$
K^o	σ = (.76±.03) mb	r_o = (.295±.006) fm	δ = (.38±.02) fm	r_o = (.380±.008) fm					
Λ		r_o = (.237±.003) fm			δ = (.115±.002) fm	σ = (.316±.008) mb	σ = (.79±.02) mb	δ = (.46±.11) fm	r_o = (.377±.004) fm
$\overline{K^o}$		r_o = (.123±.001) fm					σ = (.23±.03) mb	δ = (.11±.02) fm	r_o = (.193±.001) fm

(1) r_o is assumed equal to 1.3 fm.

In the Λ case, only the $A^{1/3}$ dependence is acceptable on a χ^2 basis. See Table 7. Listed in Table 8 are the values of various model-dependent parameters computed from the fits of straight lines to the Λ production data. Again, only the values for δ have reasonable magnitude. Because the sum of cross sections for Λ production from 850 MeV/c K^-'s incident on neutrons is about equal to that on protons,[16] the model which neglects Λ production from neutrons does not seem sensible.

In the $\overline{K}^o$ case, none of the least-square fits of straight lines to the data are acceptable on a χ^2 basis. See Table 7. Primarily to maintain consistency with the preferred models for the K^o and Λ cases, the effective rim width model is preferred in this case also. Furthermore, as shown in Table 8, this model yields a reasonable value for δ whereas the $A^{2/3}$-type models yield uncomfortably small values for r_o.

III. MONTE CARLO CALCULATIONS

A Monte Carlo computer code was written using a simple impulse approximation model for the charge-exchange production of neutral kaons and for the production of lambda hyperons from charged kaons incident on complex nuclei. Monte Carlo calculations similar to the ones described here have been performed previously in studies of intranuclear cascades initiated by protons and neutrons and pions,[18,21] but to the author's knowledge, the calculations described here are the first attempt of this type to treat the interaction and production of strange particles inside complex nuclei.

A. Nuclear Model and Input Information

The nuclear model used here was that of a Fermi gas of nucleons confined with uniform density within a volume of $(\frac{4}{3})\pi R^3$, where $R = r_o A^{1/3}$, $r_o = 1.3$ fm, and A = mass number of a given nucleus. The target nuclei studied were C, Al, Cu, Sn, and Pb. For each of these nuclei, appropriate maximum Fermi momenta were assigned.[22] After each collision inside a nucleus, the kinetic energies of the target nucleons were required to be greater than the corresponding Fermi energy, or the collision was forbidden.

The collisions with nucleons inside a nucleus were assumed to occur just as if the nucleons were free. The elementary cross sections used for the Monte Carlo calculations are shown in Table 9.

B. Course and Mechanics of the Calculation, and Results

The Monte Carlo calculations were carried out on the University of Illinois High Energy Physics I.B M. 7094. A block diagram showing the course of the Monte Carlo code is shown in Figure 11.

The incident kaons were distributed uniformly over the geometrical cross sections of the nuclei. Their distances of travel, d, in nuclear matter

Table 9

Elementary Cross Sections Used in Monte Carlo Calculations

Interaction	Cross Section (mb)	Interaction	Cross Section (mb)
$K^{(S=+1)}+N \rightarrow$ Total	14		
$K^+ + n \rightarrow K^+ + n$	7.3	$K^+ + p \rightarrow K^+ + p$	20
$\leftrightarrows K^o + p$	6.7		
$N + N \rightarrow$ Total	31		
$K^{(S=-1)}+N \rightarrow$ Total	41		
$\Lambda + N \rightarrow$ Total	20		
$\Sigma + N \rightarrow$ Total	31		
$\pi + N \rightarrow$ Total	30		
$K^- + p \rightarrow K^- + p$	23.7	$K^- + n \rightarrow K^- + n$	29.0
$\rightarrow \Lambda + \pi^c + \pi^c$	4.4	$\rightarrow \Lambda + \pi^c$	7.3
$\rightarrow \bar{K}^o + n$	4.2	$\rightarrow \Lambda + \pi^c + \pi^o$	3.0
$\rightarrow \Lambda + \pi^o$	3.7	$\rightarrow \Sigma^- + \pi^o$	1.7
$\rightarrow \Sigma^+ + \pi^c$	2.1		
$\rightarrow \Lambda + \pi^o + \pi^o$	1.4		
$\rightarrow \Sigma^- + \pi^c$	1.4		
$\bar{K}^o + n \rightarrow \bar{K}^o + n$	23.7	$\bar{K}^o + p \rightarrow \bar{K}^o + p$	29.0
$\rightarrow \Lambda + \pi^c + \pi^c$	4.4	$\rightarrow \Lambda + \pi^c$	7.3
$\rightarrow K^- + p$	4.2	$\rightarrow \Lambda + \pi^c + \pi^o$	3.0
$\rightarrow \Lambda + \pi^o$	3.7	$\rightarrow \Sigma^- + \pi^o$	1.7
$\rightarrow \Sigma^- + \pi^c$	2.1		
$\rightarrow \Lambda + \pi^o + \pi^o$	1.4		
$\rightarrow \Sigma^+ + \pi^c$	1.4		
$\Lambda + p \rightarrow \Lambda + p$	20	$\Lambda + n \rightarrow \Lambda + n$	20
$\Sigma^+ + n \rightarrow \Sigma^+ + n$	18.6	$\Sigma^+ + p \rightarrow \Sigma^+ + p$	31
$\rightarrow \Lambda + p$	12.4		
$\Sigma^- + p \rightarrow \Sigma^- + p$	18.6	$\Sigma^- + n \rightarrow \Sigma^- + n$	31
$\rightarrow \Lambda + n$	12.4		
$\pi^c + p \rightarrow \pi^c + p$	30	$\pi^c + n \rightarrow \pi^c + n$	30

Figure 11. Block diagram showing the course of the Monte Carlo codes.

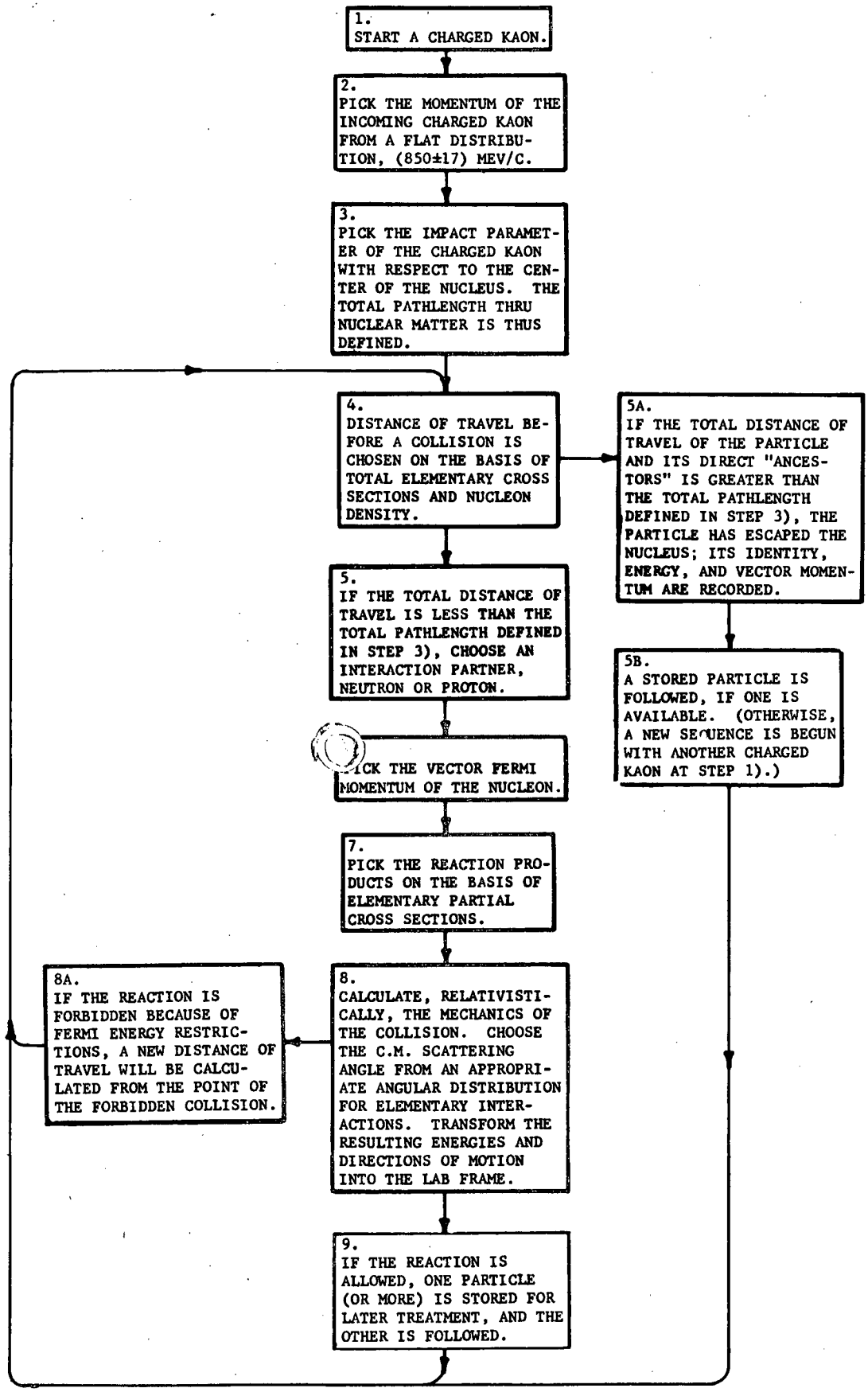
1.
START A CHARGED KAON.
2.
PICK THE MOMENTUM OF THE INCOMING CHARGED KAON FROM A FLAT DISTRIBUTION, (850±17) MEV/C.
3.
PICK THE IMPACT PARAMETER OF THE CHARGED KAON WITH RESPECT TO THE CENTER OF THE NUCLEUS. THE TOTAL PATHLENGTH THRU NUCLEAR MATTER IS THUS DEFINED.
4.
DISTANCE OF TRAVEL BEFORE A COLLISION IS CHOSEN ON THE BASIS OF TOTAL ELEMENTARY CROSS SECTIONS AND NUCLEON DENSITY.
5A.
IF THE TOTAL DISTANCE OF TRAVEL OF THE PARTICLE AND ITS DIRECT "ANCESTORS" IS GREATER THAN THE TOTAL PATHLENGTH DEFINED IN STEP 3), THE PARTICLE HAS ESCAPED THE NUCLEUS; ITS IDENTITY, ENERGY, AND VECTOR MOMENTUM ARE RECORDED.
5.
IF THE TOTAL DISTANCE OF TRAVEL IS LESS THAN THE TOTAL PATHLENGTH DEFINED IN STEP 3), CHOOSE AN INTERACTION PARTNER, NEUTRON OR PROTON.
5B.
A STORED PARTICLE IS FOLLOWED, IF ONE IS AVAILABLE. (OTHERWISE, A NEW SEQUENCE IS BEGUN WITH ANOTHER CHARGED KAON AT STEP 1).)
ICK THE VECTOR FERMI MOMENTUM OF THE NUCLEON.
7.
PICK THE REACTION PRODUCTS ON THE BASIS OF ELEMENTARY PARTIAL CROSS SECTIONS.
8A.
IF THE REACTION IS FORBIDDEN BECAUSE OF FERMI ENERGY RESTRICTIONS, A NEW DISTANCE OF TRAVEL WILL BE CALCULATED FROM THE POINT OF THE FORBIDDEN COLLISION.
8.
CALCULATE, RELATIVISTICALLY, THE MECHANICS OF THE COLLISION. CHOOSE THE C.M. SCATTERING ANGLE FROM AN APPROPRIATE ANGULAR DISTRIBUTION FOR ELEMENTARY INTERACTIONS. TRANSFORM THE RESULTING ENERGIES AND DIRECTIONS OF MOTION INTO THE LAB FRAME.
9.
IF THE REACTION IS ALLOWED, ONE PARTICLE (OR MORE) IS STORED FOR LATER TREATMENT, AND THE OTHER IS FOLLOWED.

were computed according to the formula

$$d = -\lambda \ln \chi,$$

where χ is a random number between zero and 1, and λ was the mean-free-path of the kaons in nuclear matter,

$$\lambda = \frac{1}{n\sigma} = \frac{4\pi r_o^3}{3\sigma(KN)} ;$$

and $\sigma(KN)$ was the total kaon-nucleon cross section. The distances of travel of other particles in nuclear matter were computed in the same way, with the appropriate total particle-nucleon cross sections substituted for $\sigma(KN)$.

The percentage of kaons that should pass through a spherical nucleus without interacting is (ignoring a small correction for Pauli exclusion effects)

$$P = \frac{\int_0^{2\pi} r d\phi \int_0^R \exp[-2(R^2-r^2)^{\frac{1}{2}}/\lambda] dr}{\int_0^{2\pi} r d\phi \int_0^R dr}$$

$$= \frac{\lambda^2}{2R^2}\left[1-e^{-\frac{2R}{\lambda}}\left(\frac{2R}{\lambda}+1\right)\right] ,$$

where R is the nuclear radius. This expression provides a check on part of the Monte Carlo program. It predicts percentages only about 3% lower than the percentage of non-interacting kaons in the Monte Carlo results.

A typical run consisted of 4000 K^+'s or 8000 K^-'s incident on each of the five nuclei studied. The type, energies, and vector momenta of all of the escaping particles was recorded on magnetic tapes for later analysis by University of Illinois-Cern SUMX routines.

There were significant differences in the complexities of the computer codes which handled the K^+ and the K^- incident particles; therefore,

they will be discussed separately.

1. K^+

The code for the K^+ runs was the simpler of the two. For K^+ incident with ~850 MeV/c momentum on complex nuclei, the only interactions of importance are elastic scattering and charge-exchange.[15]

The elementary particle cross sections which were used in the program were the total kaon-nucleon and the total nucleon-nucleon and the K^+n charge-exchange cross sections.

The C.M. angular distributions of all the elementary collisions were given by the angular distribution appropriate to $K^+n \rightarrow K^op$ in the center-of-mass frame.[22] This was not considered a serious fault in the code, since the angular distributions of the neutral kaons were the only angular distributions of major importance.

For comparison with the experimental data, cross sections were computed for the total production of K^o's from complex nuclei relative to the cross section on carbon. The relative cross sections were computed according to the formula

$$\frac{\sigma_N}{\sigma_C} = \frac{\#K^o{}_N}{\#K^o{}_C} \frac{A_N^{2/3}}{A_C^{2/3}} ,$$

where N stands for the nuclear type, $\#K^o$ was the total number of K^o's produced, and A was the mass number of the nucleus. (For the K^+ and K^- studies, a total of 4000 and 8000 charged kaons, respectively, were incident on each nuclear type.) Then two cuts, which corresponded to the real experimental situation, were made on the Monte Carlo data. Only K^o's with momentum > 400 MeV/c and with production angles < 1.05 radians were accepted, and the relative cross sections were recomputed. The results of both these computations and the

appropriate statistical error bars are shown in Figure 12. Also shown in Figure 12 are the experimental data points. It is clear that the Monte Carlo cross sections with no cuts, which show a linear dependence on the number of neutrons in the complex nuclei from carbon through lead, do not fit the experimental data. Interestingly, however, the Monte Carlo calculations with cuts do match the data well.

Other angle cuts, .84 rad. and 1.26 rad., were tried, resulting in less than one standard deviation change in the relative cross sections. Other momentum cuts were tried. A 300 MeV/c cut resulted in increases in the relative cross sections by about one standard deviation; a 500 MeV/c cut resulted in decreases by about one standard deviation.

Keeping track of events in which the K^o's were accompanied by energetic protons that might have vetoed the events in a real experiment gave results which were the same, within statistics, as those for which no attention was paid to the protons.

When the total KN cross section was changed from 14 mb to 20 mb, the relative cross sections tended toward smaller values. The relative cross section for lead was more than two standard deviations smaller for $\sigma(KN) = 20$ mb than for $\sigma(KN) = 14$ mb.

2. K^-

The code for the K^- runs was complicated by the fact that so many channels of interaction are available for negative kaons incident at 850 MeV/c on protons or neutrons. In all, 32 possible interactions were allowed within the K^- code. See Table 9.

Also, there was provision in the K^- code for four different angular distributions in the center-of-mass frame. One was appropriate for elastic

Figure 12. Comparison of K^+ Monte Carlo results to experimental data.

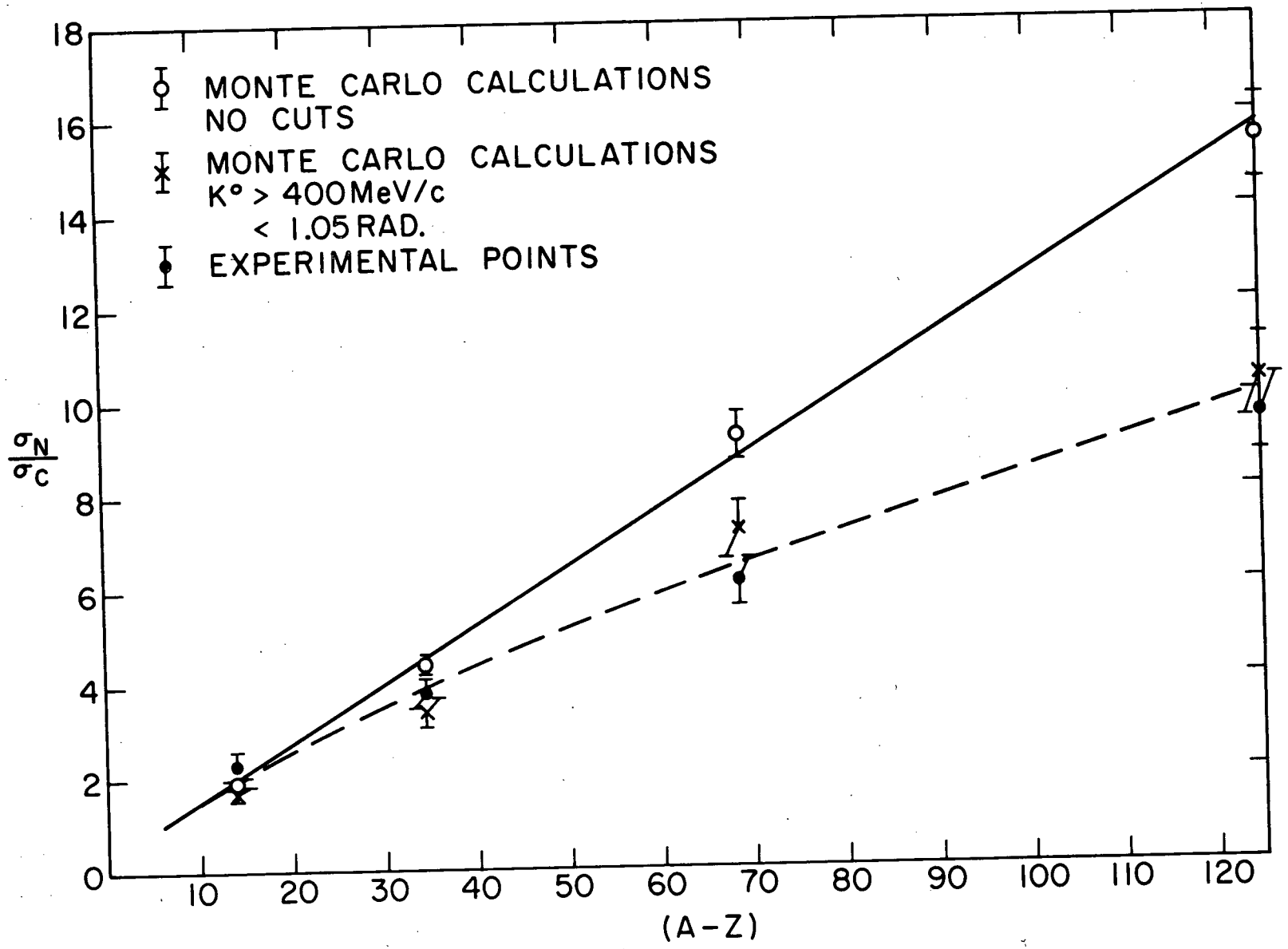
MONTE CARLO CALCULATIONS
NO CUTS
MONTE CARLO CALCULATIONS
K° > 400MeV/c
< 1.05 RAD.
EXPERIMENTAL POINTS
σN/σC
(A-Z)
0
2
4
6
8
10
12
14
16
18
10
20
30
40
50
60
70
80
90
100
110
120

scattering of kaons from nucleons[12]; another was appropriate for kaon charge-exchange on nucleons[12]; a third was for production of lambdas with one pion from kaons on nucleons[13]; and the fourth, a uniform distribution, was used for all the other interactions.

a. $K^- \rightarrow \overline{K}^o$

In order to compare the Monte Carlo production of $\overline{K}^o$'s to the experimental data, cross sections for the total $\overline{K}^o$ production from complex nuclei, relative to the production from carbon, were computed as described in section III.B.1. Again, the Monte Carlo cross sections with no cuts do not fit the data. Neither, in this case, do they exhibit a linear dependence on the number of protons in the complex nuclei. See Figure 13. The lack of linearity with Z is the result of two factors. One is that the mean-free path of K^-'s in nuclear matter is about 1/3 of that for K^+'s, so that the production of $\overline{K}^o$'s tends to "saturate" earlier as a function of Z than the production of K^o's as a function of (A-Z). The other factor is the "competition", in succeeding collisions of the $\overline{K}^o$'s, from the Λ and Σ production channels for the one unit of negative strangeness provided by each incident K^-.

However, as in the K^+ case, when relative cross sections were computed from just the $\overline{K}^o$'s that had momenta > 400 MeV/c and production angles < 1.05 radians, the agreement of the Monte Carlo results with the experimental data, displayed in Figure 13, is satisfactory.

b. $K^- \rightarrow \Lambda$

Lastly, efforts were made to understand the lambda yields, for which there were many production channels available. See Table 9. In this case, the agreement between the Monte Carlo results and the experimental results was not very good.

Figure 13. Comparison of $K^- \rightarrow K^o$ Monte Carlo results to experimental data.

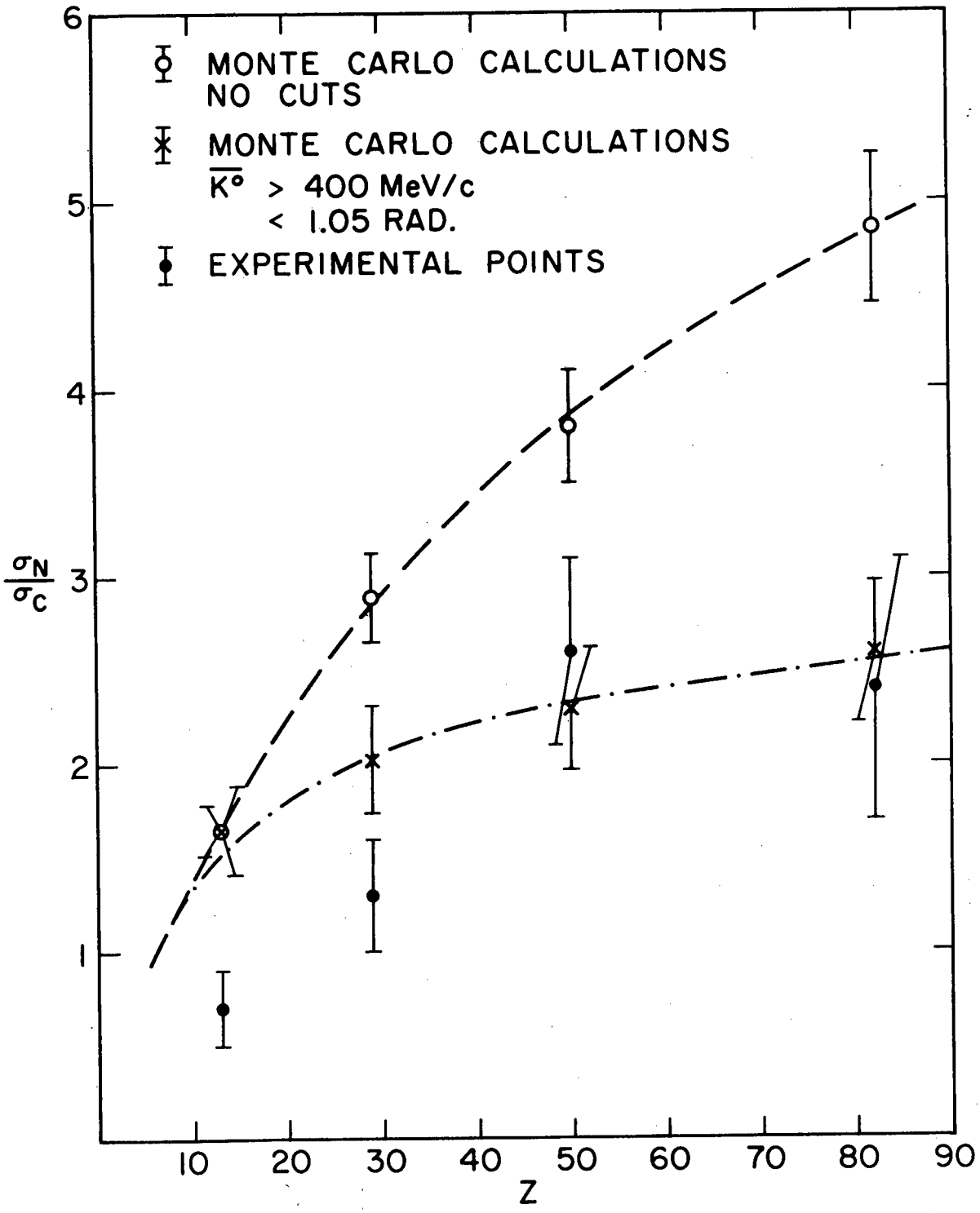
MONTE CARLO CALCULATIONS
NO CUTS
MONTE CARLO CALCULATIONS
$\overline{K^0}$ > 400 MeV/c
< 1.05 RAD.
EXPERIMENTAL POINTS
$\frac{\sigma_N}{\sigma_C}$
Z
6
5
4
3
2
1
10
20
30
40
50
60
70
80
90

The relative cross sections for the total production of lambdas were computed in the same way as described for K^o's. In Figure 14, the relative cross sections have been plotted versus A, since lambdas can be produced by 850 MeV/c K^-'s on neutrons with about the same cross section as on protons.[16] The dependence is not quite linear, but the Monte Carlo cross sections do increase sharply with A, with the cross section for Λ production about twelve times larger from lead than from carbon.

In contrast, the experimental data indicate that the cross section for Λ production from lead is only $2\frac{1}{2}$-3 times larger than that from carbon.

As in the K^o and $\overline{K}^o$ cases, cuts corresponding to real experimental detection requirements were made on the Monte Carlo data, and the relative cross sections were re-computed. When the lambdas were required to have momentum > 700 MeV/c and production angles < 1.05 radians, the relative cross sections "turn over" rather sharply, suggesting the even more drastic trend of the experimental data, as shown in Figure 14. Still, there remains about a factor of 2 difference between the experimental results for lead and the Monte Carlo results.

As in the case of K^o production, it was found that varying the production angle cut by $\pm$ .21 rad. resulted in less than one standard deviation changes in the relative cross sections. Other momentum cuts of 600 MeV/c and 800 MeV/c resulted, respectively, in increases and decreases in the relative cross sections by about one standard deviation.

For K^o and $\overline{K}^o$ production it was found that keeping track of Monte Carlo events in which a proton was present, with proper direction and sufficient energy to register in imaginary anti counters surrounding the target, made no significant difference in the relative cross sections. For lambda production, however, it was expected that charged pions would have a significant

Figure 14. Comparison of $K^- \rightarrow \Lambda$ Monte Carlo results to experimental data.

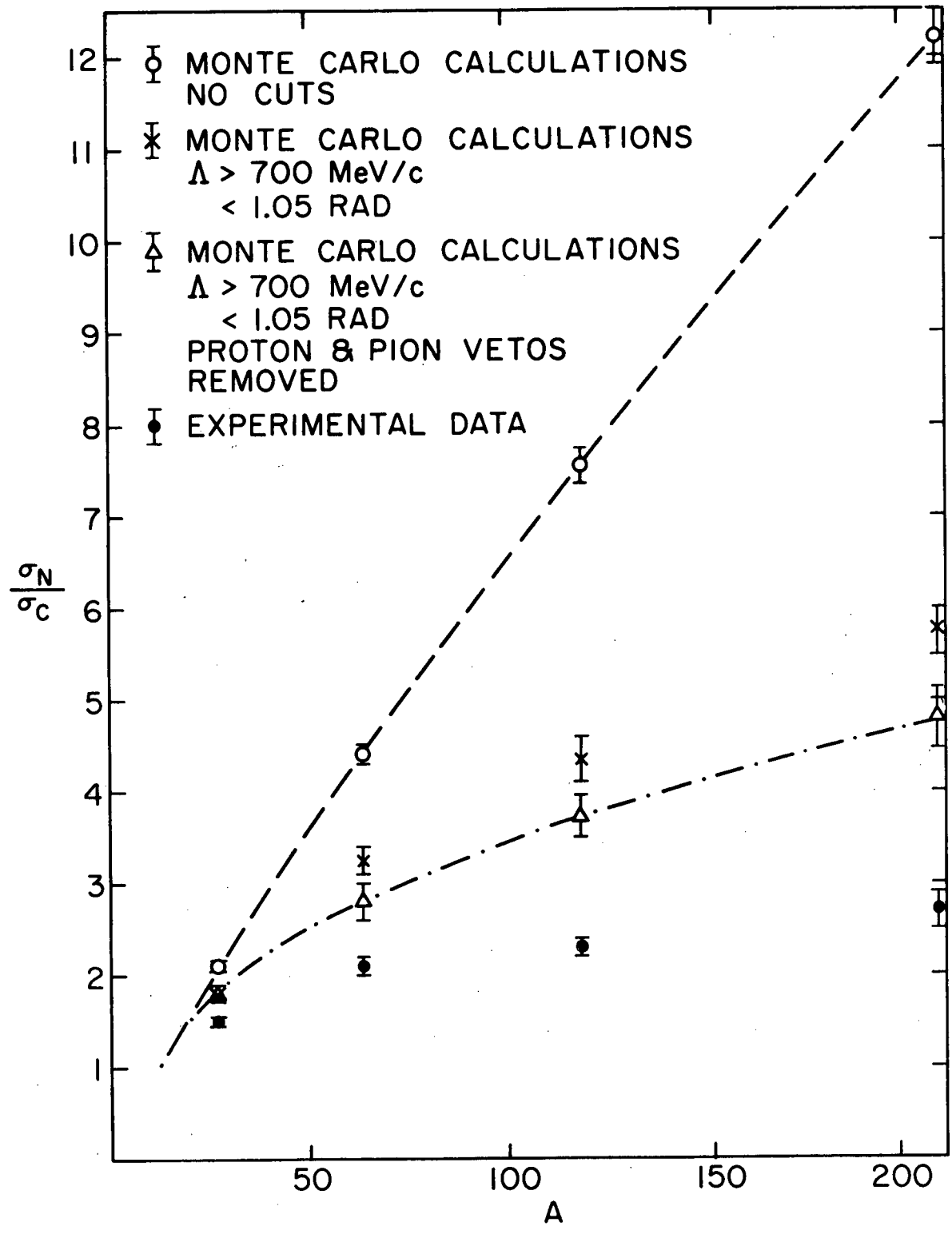
MONTE CARLO CALCULATIONS
NO CUTS
MONTE CARLO CALCULATIONS
Λ > 700 MeV/c
< 1.05 RAD
MONTE CARLO CALCULATIONS
Λ > 700 MeV/c
< 1.05 RAD
PROTON & PION VETOS
REMOVED
EXPERIMENTAL DATA
σN/σC
A
12
11
10
9
8
7
6
5
4
3
2
1
50
100
150
200

effect when attention was paid to which events they could have vetoed. When events which could have been vetoed by charged pions, or protons, were removed from the Λ production events surviving the momentum and production angle cuts, the results shown in Figure 14 were obtained. The pion and proton vetoes had a 2-3 standard deviation effect in decreasing the relative cross sections for nuclei heavier than aluminum.

Still, the Monte Carlo relative cross sections for lambda production do not agree well with the experimental cross sections. The neutral pions that are often produced with lambdas, as indicated in Table 9, provide a possible explanation for much of the discrepancy. About 41% of all the lambdas produced by 850 MeV/c negative kaon interactions on protons or neutrons are produced together with one or more neutral pions. The neutral pions decay very rapidly into two γ's which can convert into e^+e^- pairs while still in the target.

The percentage of the γ's that convert in the lead target, for example, is much greater than in the carbon target, because even though both targets contained about 0.1 collision lengths, they differed significantly in pair-production lengths. The pair-production lengths that each target presented to the beam are shown in Table 10, together with the probability that a photon would convert to e^+e^- in passing through the entire length of the target. To obtain a rough estimate of the size of the effect, it was assumed that each pion gave one photon which would veto a lambda event if it converted when passing through the entire target length. The relative Monte Carlo cross sections after the cuts and after the removal of proton and pion vetoes were adjusted according to the formula

$$\left(\frac{\sigma_N^{\Lambda}}{\sigma_C^{\Lambda}}\right)' = \frac{\sigma_N^{\Lambda}}{\sigma_C^{\Lambda}} \frac{[1-R\cdot P_N]}{[1-R\cdot P_C]} \quad ,$$

Table 10

Target	Pair-Production Lengths	Conversion Probability	$\frac{\sigma_N^\Lambda}{\sigma_C^\Lambda}$	$\left(\frac{\sigma_N^\Lambda}{\sigma_C^\Lambda}\right)'$	$\frac{\sigma_N^\Lambda}{\sigma_C^\Lambda}$ (EXPT.)
Carbon	.107	.101	1.0	1.0	1.0
Aluminum	.269	.236	1.8	1.7	$1.50 \pm .05$
Copper	.793	.545	2.8	2.3	$2.1 \pm .1$
Tin	1.32	.733	3.7	2.7	$2.3 \pm .1$
Lead	1.99	.863	4.8	3.2	$2.7 \pm .2$

where R is the fraction of Λ's produced together with π^o's, and P is the conversion probability. The values of $(\sigma_N^{\Lambda}/\sigma_C^{\Lambda})'$ and the experimental values of the relative cross sections are tabulated in Table 10. With the rough adjustments described above, the Monte Carlo relative cross sections for Λ production are very near the experimental values.

IV. SUMMARY AND CONCLUSIONS

Measurements of cross sections have been presented for the charge-exchange production of K^o and $\overline{K}^o$ mesons and for Λ production from charged kaons incident on several complex nuclear targets.

An "effective rim width" model for the hydrogen-like production of the neutral kaons and lambdas has been applied to the experimental data; and from least-squares fits of the model to the data, values of the effective rim width parameter, δ, have been derived.

The values of δ probably are dependent on the partial production cross sections and on the mean-free-paths of the incident and product particles in nuclear matter. Therefore, for other incident energies or other incident or product particles than those discussed in this thesis, the values found here for δ would not be likely to be very useful in estimating expected cross sections from complex nuclei, though the model itself should remain applicable.

An $A^{2/3}$-type model was found to fit the data for K^o and $\overline{K}^o$ cross sections as well as the "effective rim width" model, on a χ^2-basis. However, the $A^{2/3}$ models led to unusually small values for the nuclear unit radius r_o.

A Monte Carlo study of the production of neutral kaons and lambdas from charged kaons incident on complex nuclei was done. In general, the total particle yields from the Monte Carlo programs lead to cross sections, relative to carbon, that were much larger than those found experimentally. However, when the $>$ 400 MeV/c momentum and $>$ 1.05 RAD. production angle cuts that were present in the experimental data were applied to the Monte Carlo results, as on pages 59 and 63, the two were in reasonably good agreement, for neutral kaon production.

One very interesting aspect of the Monte Carlo study is best illustrated in the K^o results. Before the cuts are applied, the K^o production shows

an essentially linear dependence on (A-Z). After the cuts corresponding to experimental detection requirements were applied, the results show a curved dependence similar to the experimental data which were in agreement with either an $A^{2/3}$- or $A^{1/3}$-type dependence. In other words, the experimental efficiency and cuts may have led to the $A^{2/3}$-type dependence for the experimental cross sections.

One of the main motivations for this experiment was to determine which target materials were best for copious charge-exchange production of neutral kaons, with the restriction that the target would be limited to some maximum length. For Experiment E-256[1/] the maximum target length was about 7 centimeters.

The ratio of the number of K^o's produced to the number of K^+'s incident on the target of material N is given by

$$\left(\frac{\#K^o}{\#K^+}\right)_N = \frac{\sigma_N(K^+ + {}_Z N^A \rightarrow K^o + X)}{\sigma_T} \left(1 - e^{-n\sigma_T t}\right)$$

where n is the density of nuclei, and t is the target thickness; σ_T is assumed equal to $\pi r_o^2 A^{2/3}$ with r_o = 1.3 fm; and the value of σ_N is read from the straight line in Figure 8. Similar expressions give the ratio of K^o's and Λ's to incident K^-'s, with the values of σ_N read from Figures 10 and 9, respectively.

In Figure 15, the number of K^o,$\bar{K}^o$, and Λ particles produced per incident charged kaon, as measured in this experiment, are plotted for a 7 cm target length. It is clear that the greatest numbers of the particles of interest could be produced on copper.

Another important concern for E-256 was to keep the background from Λ events and ill-defined, or "JUNK", events as low as possible in the $\bar{K}^o$ sample. It was found that the best $\bar{K}^o/(\Lambda+\text{JUNK})$ detection ratio was obtained for carbon, the target for which Λ/K^- was lowest.

Figure 15. Number of K^o, $\overline{K}^o$, and Λ particles produced per incident charged kaon, for a 7 cm target length.

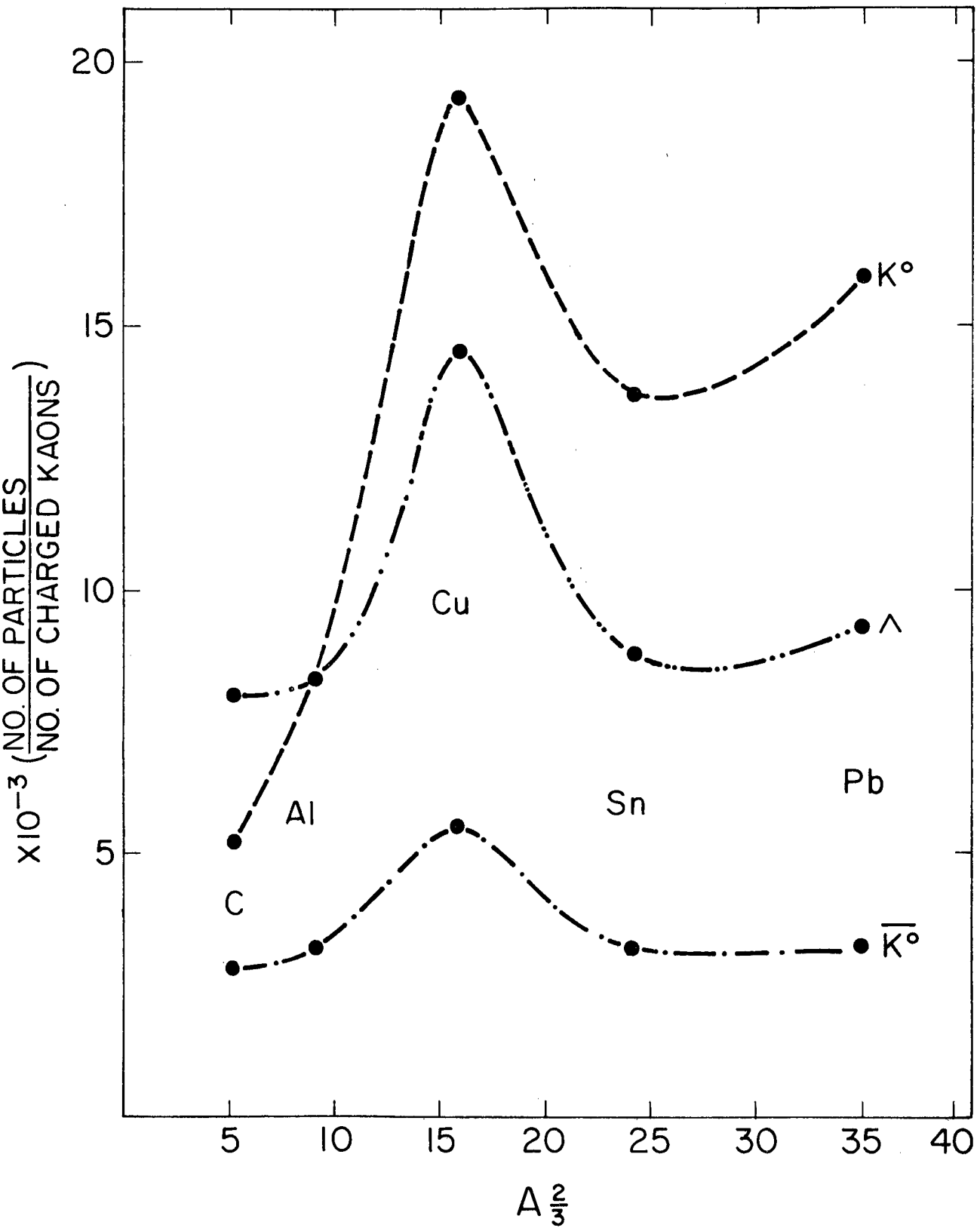
20
15
10
5
$\times 10^{-3}$ (NO. OF PARTICLES / NO. OF CHARGED KAONS)
K°
Λ
$\overline{K}°$
Al
Cu
Sn
Pb
C
5
10
15
20
25
30
35
40
$A^{\frac{2}{3}}$

Therefore, it was decided to take all of the $\bar{K}^o$ data for E-256 with a carbon target, with which about 3×10^{-3} $\bar{K}^o$'s and 8×10^{-3} Λ's per incident K^- were produced. In order not to frequently disturb the position of the target, most of the K^o data was also taken with a carbon target, yielding about 5×10^{-3} K^o's per incident K^+. Some of the K^o data was taken with a copper target, with which K^o production was best: about 19×10^{-3} per incident K^+.

For experimentalists who may wish to estimate particle yields in different experimental situations, a Monte Carlo technique similar to the one described in this thesis is probably indispensible. The Monte Carlo code could be improved by the inclusion of energy-dependent total cross sections and the careful treatment of as many differential cross sections (angular distributions) as are available. Furthermore, this thesis has shown that it is very important to incorporate the Monte Carlo code for the nuclear interactions into a larger program that includes the effects of all experimental constraints and cuts.

APPENDIX A

MAGNETOSTRICTIVE DETECTION APPARATUS

Each of the wire spark chambers had two magnetostrictive wire pickup wands attached to it, one for the high voltage plane and one for the ground plane of the chamber.

The wands were cut from 3/16" flat aluminum sheet. Each wand was $\frac{1}{2}$" wide, and the length varied to fit the chamber for which it was intended. A cross section, perpendicular to the length of the wand, is shown in Figure 16.

A 3/64"X.030" groove was cut along the entire length of the wand. Into this groove was fitted a piece of "PE 50" .023"X.038" polyethylene tubing, and a length of .015"X.004" magnetostrictive ribbon was threaded through the tubing. The ribbon was purchased from the Wilbur B Driver Co., Newark, New Jersey and carried the trade name "Remendur P."

The wand, tubing, and ribbon assembly were wrapped with one layer of .002" Mylar tape.

At one end of the wand, the ribbon was clamped and damped between two tiny pieces or rubber, to prevent reflections of acoustic signals from the end of the ribbon.

At the other end of the wand a Science Accessories Corp. (S.A.C.) preamplifier, model 1001, in an aluminum housing, was attached. The magnetostrictive ribbon passed through a hole in the preamp housing and through a plastic sleeve wound with a wire coil positioned over a small permanent magnet. The coil on the plastic sleeve consisted of 6 turns of 6 mil dia. copper wire. After passing through the coil the ribbon was clamped and damped between small felt and rubber pads. See Figure 17.

Figure 16. Cross section of pickup wand assembly.

Figure 17. Details of magnetostrictive pickup and damping.

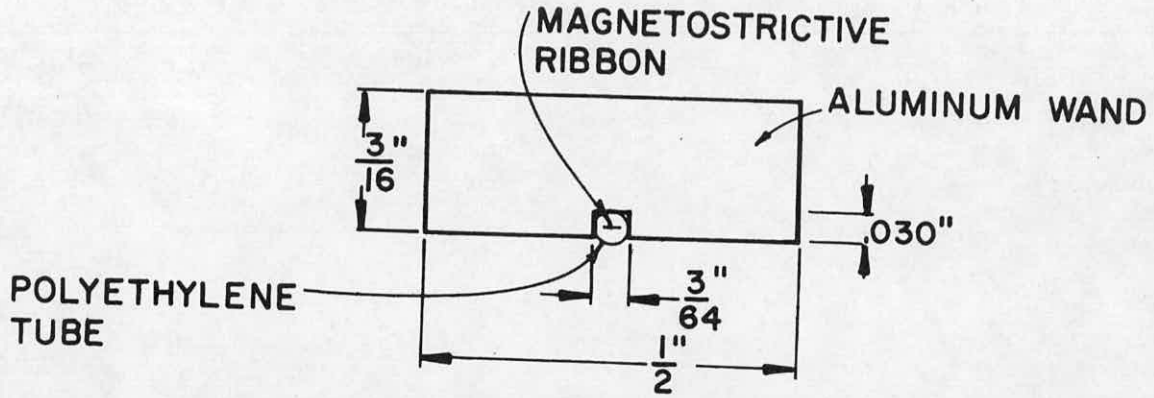
MAGNETOSTRICTIVE
RIBBON
ALUMINUM WAND
3/16"
.030"
POLYETHYLENE
TUBE
3/64"
1/2"

Fig 16

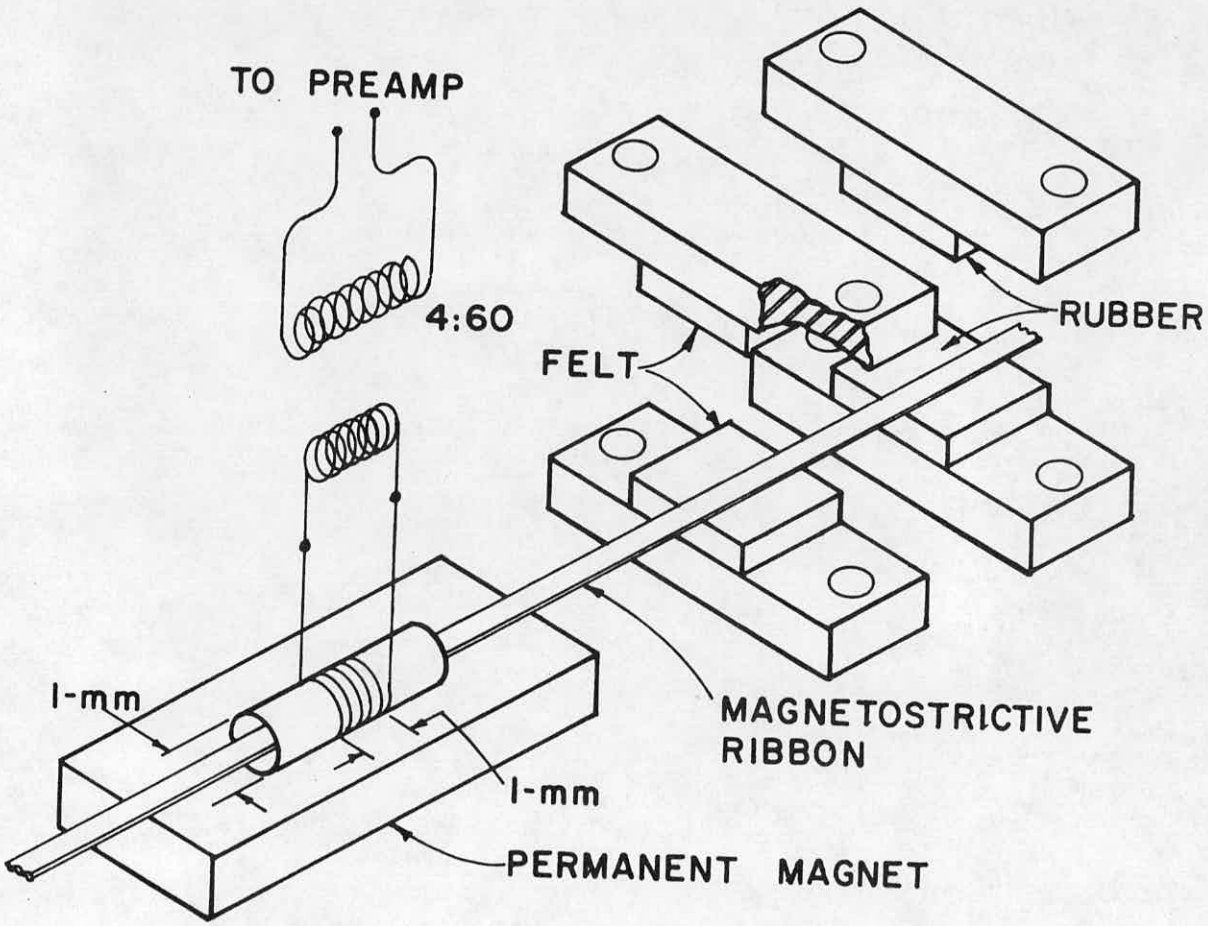
TO PREAMP
4:60
FELT
RUBBER
1-mm
1-mm
MAGNETOSTRICTIVE
RIBBON
PERMANENT MAGNET

Fig 17

The coil was attached to a step-up transformer, 4 turns: 60 turns of 15 mil dia. copper wire, wound on a 3/8" O.D. ferrite core, which was connected to the input stage of the preamp. See Figure 18 for a circuit diagram of the preamplifier.

With a pickup wand constructed as described above, tripolar pulses of the general shape and size shown in Figure 19 were typically produced when the wand was placed directly over a 10 mil copper wire carrying current from the discharge through 220Ω of 2000 pfd at 5 KV.

Attenuation of the magnetostrictive pulses over the length of the longest wands used for E-256, 55 inches, was negligible (< 10%) so long as one was careful not to induce pulses in the last $\frac{1}{4}$" to $\frac{1}{2}$" of the wand at the end opposite the preamp. Within that distance attenuation of any pulse was usually severe due to contact between the magnetostrictive ribbon and the polyethylene tubing.

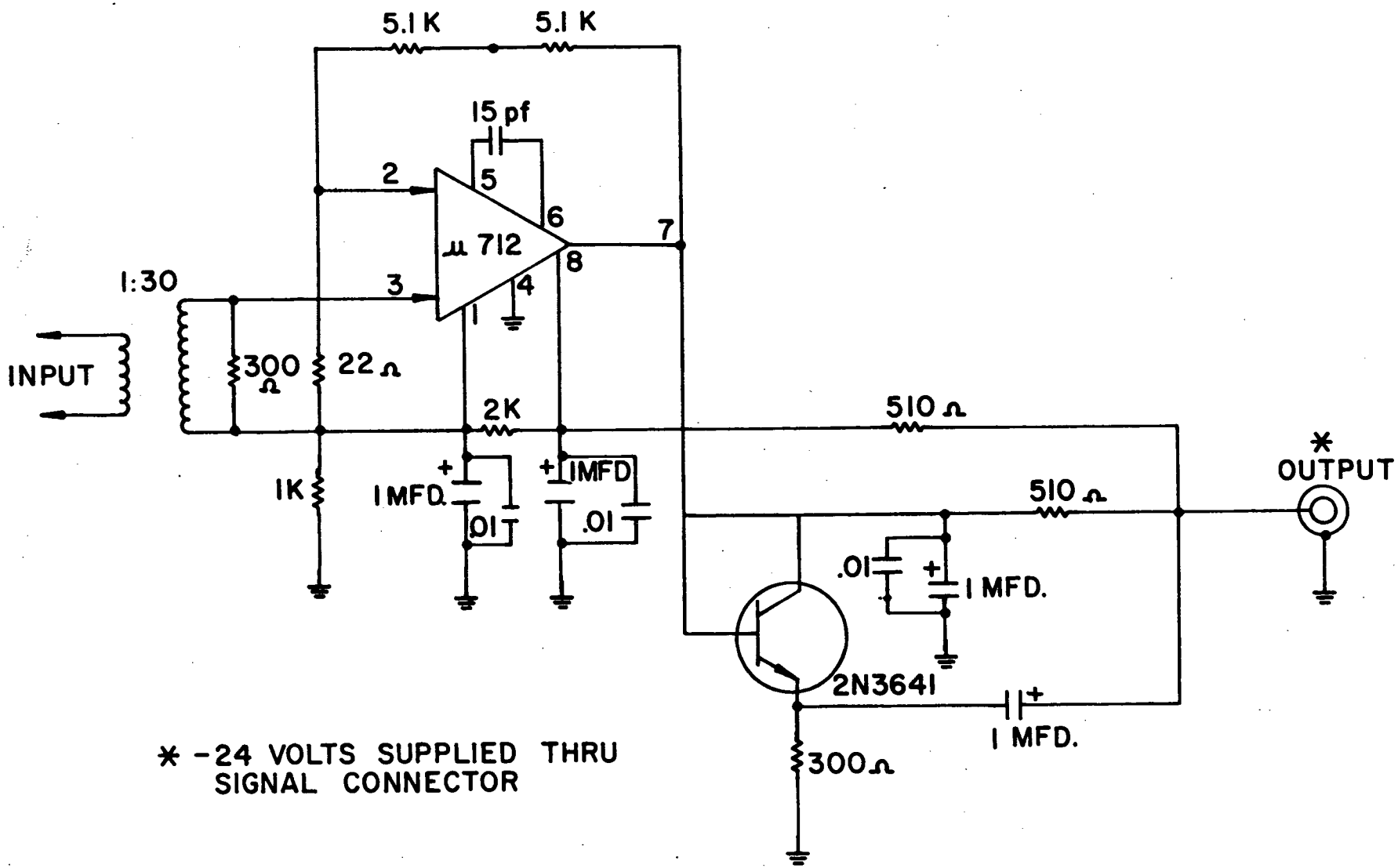

* -24 VOLTS SUPPLIED THRU SIGNAL CONNECTOR

Figure 19. Typical tripolar pulse from a magnetostrictive pickup wand.

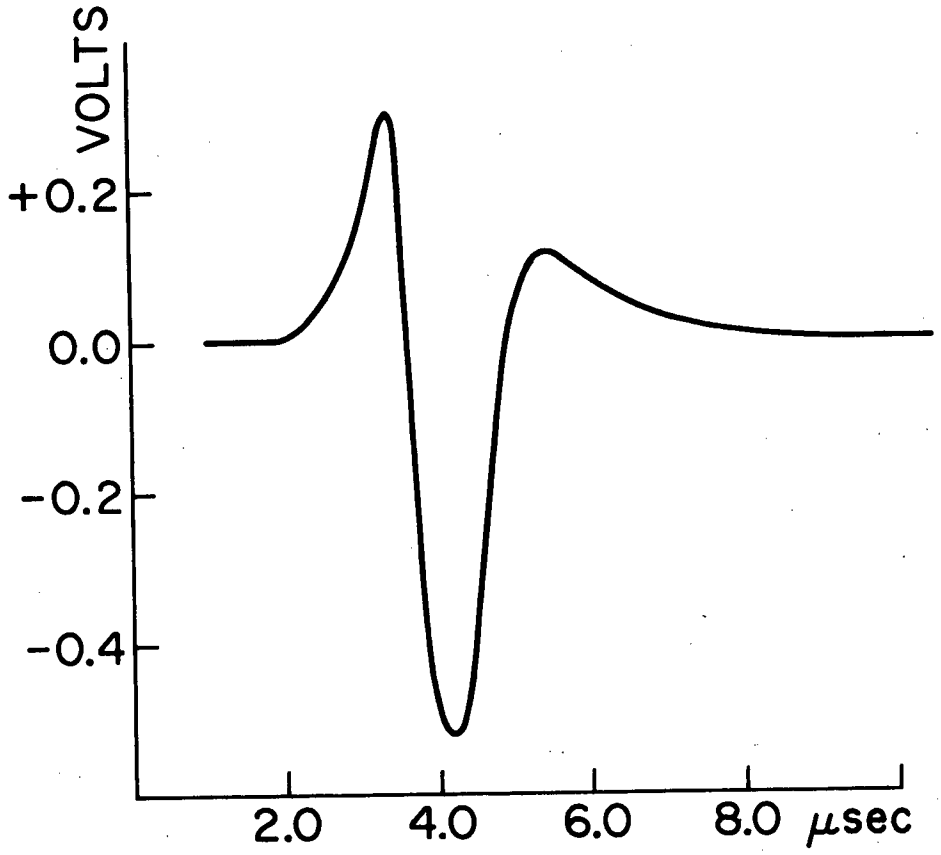
VOLTS
+0.2
0.0
-0.2
-0.4
2.0
4.0
6.0
8.0 μsec

REFERENCES

1. A. Wattenberg, R. Brown, M. Gormley, L. Koester, J. H. Smith, D. Banner, J. Frank, S. Raither. Argonne National Laboratory Z.G S. Proposal for Experiment E-256. (unpublished)

2. See the Argonne National Laboratory Z.G.S. Users Handbook for a description of this magnet.

3. J. W. Gardner and D. Whiteside, TRAMP, NIRL/M/21, 1961.

4. Owen Chamberlain, Ann. Rev. Nucl. Sci. 10, 161 (1960).

5. D. Banner and I. Spirn, Argonne National Laboratory. High Energy Physics internal report, March 26, 1971. (unpublished)

6. J. Frank, Ph.D. thesis, University of Illinois at Urbana-Champaign, 1972. (unpublished)

7. S. Raither, Ph.D. thesis, University of Illinois at Urbana-Champaign, 1972. (unpublished)

8. V. Perez-Mendez and J. M. Pfab, Nucl. Instr. and Methods 33, 141 (1965).

9. V. Perez-Mendez, T. J. Devlin, J. Solomon, and J. F Droege, Nucl. Instr. and Methods 46, 197 (1967).

10. M. L. Marshak and S. M. Pruss, Nucl. Instr. and Methods 62, 295 (1968).

11. Rev. of Modern Phys. 43, No. 2, Part II, Supplement, April (1971).

12. L. Bertanza, A. Bigi, R. Carrara, R. Casali, R. Pazzi, D. Berley, E. L. Hart, D. C. Rahm, W. J. Willis, S. S. Yamamoto, and N. S. Wong, Phys. Rev. 177, 2036 (1969).

13. R. Armenteros, M. Ferro-Luzzi, D. W. G. S. Leith, R. Levi-Setti, A. Minten, R. D. Tripp, H. Filthuth, V. Hepp, E. Kluge, H. Schneider, R. Barlontand, P. Granet, J. Meyer, and J.-P. Porte, Nuc. Phys. B8, 233 (1968).

14. P. L. Bastien and J. Peter Berge, Phys. Rev. Letters 10, 188 (1963).

15. E. Flamino, J. D. Hansen, D. R. O. Morrison, and N. Tovey, "Compilation of Cross Sections III - K^+ Induced Reactions," CERN/HERA 70-4, September, 1970.

16. E. Flamino, J. D. Hansen, D. R. O. Morrison, and N. Tovey, "Compilation of Cross Sections V - K^- Induced Reactions," CERN/HERA 70-6, October, 1970.

17. Robley D. Evans, The Atomic Nucleus, McGraw-Hill Book Co., Inc., 1955, pp. 42-43.

18. N. Metropolis, R. Bivins, M. Storm, A. Turkevich, J M. Miller, and G. Friedlander, Phys. Rev. 110, 185 (1958); Phys. Rev. 110, 204 (1958).

19. Implicit here is the assumption that the nuclear unit radius for neutrons is about the same as that for protons. See H. J Körner and J. P Schiffer, Phys. Rev. Letters 27, 1457 (1971).

20. S. Frankel, V. Highland, T. Sloan, O. Van Dyck, and W. Wales, Phys. Rev. 177, 2113 (1969).

21. S Thakore, A. C. Melissinos, and J. Tinlot, "7070 Program for a Monte Carlo Calculation of a Nuclear Cascade," The University of Rochester, Department of Physics and Astronomy, NYO-10132.

22. E. J. Moniz, I. Sick, R. R. Whitney, J. R. Ficenec, R. D. Kephart, and W. P. Trower, Phys. Rev. Letters 26, 445 (1971).

23. L. R. Price, N. Barash-Schmidt, O. Benary, R. W. Bland, A. H. Rosenfeld, and C. G. Wohl, "A Compilation of K^+N Reactions," UCRL-20000 K^+N, September, 1969.

VITA

David Lee Banner was [redacted] He graduated from North Kansas City High School, North Kansas City, Missouri, in June, 1960. He received a Bachelor of Science degree "with highest distinction" from Purdue University in June, 1964. While at Purdue, he held an Alfred P. Sloan Foundation scholarship for four years. He spent the 1964-65 academic year as a U. S. Churchill Scholar at Churchill College, Cambridge University, England. He entered the University of Illinois in September, 1965, and received his Master of Science degree in physics in August, 1966. While at the University of Illinois he held a University Fellowship and teaching and research assistantships.

He is a member of the American Physical Society, Sigma Pi Sigma, and Phi Eta Sigma.